V2-Directed Vaccine-like Antibodies from HIV-1 Infection Identify an Additional K169-Binding Light Chain Motif with Broad ADCC Activity

Charmaine van Eeden[1,2,10], **Constantinos Kurt Wibmer**[1,2,10,11], **Cathrine Scheepers**[1,2], **Simone I. Richardson**[1,2], **Molati Nonyane**[1], **Bronwen Lambson**[1,2], **Nonhlanhla N. Mkhize**[1,2], **Balakrishnan Vijayakumar**[3], **Zizhang Sheng**[4,5], **Sherry Stanfield-Oakley**[6], **Jinal N. Bhiman**[1,2,11], **Valerie Bekker**[1], **Tandile Hermanus**[1], **Batsirai Mabvakure**[1,2], **Arshad Ismail**[1], **M. Anthony Moody**[6], **Kevin Wiehe**[6], **Nigel Garrett**[7], **Salim Abdool Karim**[7], **Heini Dirr**[3], **Manuel A. Fernandes**[8], **Yasien Sayed**[3], **Lawrence Shapiro**[4,9], **Guido Ferrari**[6], **Barton F. Haynes**[6], **Penny L. Moore**[1,2,7], and **Lynn Morris**[1,2,7,12,*]

[1]National Institute for Communicable Diseases of the National Health Laboratory Service, Johannesburg 2131, South Africa

[2]Faculty of Health Sciences, University of the Witwatersrand, Johannesburg 2000, South Africa

[3]Protein Structure-Function Research Unit, University of the Witwatersrand, Johannesburg 2000, South Africa

[4]Department of Biochemistry and Molecular Biophysics, Columbia University, New York, NY 10027, USA

[5]Department of Systems Biology, Zukerman Mind Brain Behavior Institute, Columbia University, New York, NY 10027, USA

[6]Duke Human Vaccine Institute, Duke University, Durham, NC 27710, USA

[7]Centre for the AIDS Programme of Research in South Africa (CAPRISA), University of KwaZulu Natal, Durban 4041, South Africa

[8]Molecular Sciences Institute, School of Chemistry, University of the Witwatersrand, Johannesburg 2000, South Africa

*Correspondence: lynnm@nicd.ac.za.

[9]Vaccine Research Center, National Institute of Allergy and Infectious Diseases, NIH, Bethesda, MD 20892-9806, USA

[10]These authors contributed equally

[11]Present address: The Scripps Research Institute, La Jolla, CA 92037, USA

[12]Lead Contact

SUMMARY

Antibodies that bind residue K169 in the V2 region of the HIV-1 envelope correlated with reduced risk of infection in the RV144 vaccine trial but were restricted to two ED-motif-encoding light chain genes. Here, we identify an HIV-infected donor with high-titer V2 peptide-binding antibodies and isolate two antibody lineages (CAP228-16H/19F and CAP228–3D) that mediate potent antibody-dependent cell-mediated cytotoxicity (ADCC). Both lineages use the IGHV5–51 heavy chain germline gene, similar to the RV144 antibody CH58, but one lineage (CAP228-16H/19F) uses a light chain without the ED motif. A cocrystal structure of CAP228-16H bound to a V2 peptide identified a IGLV3–21 gene-encoded DDxD motif that is used to bind K169, with a mechanism that allows CAP228-16H to recognize more globally relevant V2 immunotypes. Overall, these data further our understanding of the development of cross-reactive, V2-binding, antiviral antibodies and effectively expand the human light chain repertoire able to respond to RV144-like immunogens.

In Brief

V2-directed antibodies from the RV144 vaccine trial correlated with reduced HIV-1 infection risk but exhibited restricted light chain gene usage. Here, van Eeden et al. isolate similar antibodies from an HIV-1-infected individual and identify a third V2-reactive light chain gene, increasing the antibody repertoire potentially elicited by vaccination.

Graphical Abstract
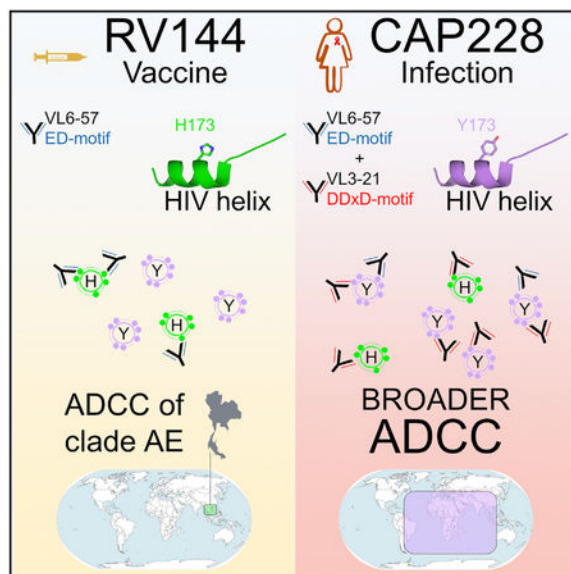
INTRODUCTION

The RV144 vaccine trial was the first HIV-1 phase III human clinical trial to show a favorable outcome, with a moderate 31.2% efficacy (Rerks-Ngarm et al., 2009). A case-control analysis showed that cross-reactive binding antibodies specific for the V2 region of HIV-1 Env correlated inversely with infection risk (Haynes et al., 2012). Selection pressure was identified at positions 169 and 181 in V2, and vaccine efficacy was greater (~48%) when viruses had a matched V2 K169 residue (Rolland et al., 2012). The V2 region of Env is also a target for broadly neutralizing antibodies (bNAbs), and position 169 is often a mutational hot spot for antibody escape during infection (Moore et al., 2011; Wibmer et al., 2013, 2015). However, since vaccine-induced V2 antibodies were only able to neutralize sensitive tier 1 virus strains, exactly how these antibodies contributed to reduced infection rates remains unknown (Rerks-Ngarm et al., 2009).

The isolation of several monoclonal antibodies (mAbs) from RV144 vaccinees that bound short, linear, V2 peptide epitopes spanning positions 166–182 of Env, have provided possible mechanisms of action. These V2 mAbs were able to mediate antibody-dependent cell-mediated cytotoxicity (ADCC) against CD4+ target cells coated in Env derived from breakthrough infections (Liao et al., 2013) and subtype AE HIV-1 CM235 infectious molecular clone-infected target cells (Pollara et al., 2014). Among RV144 vaccinees, 28% had V2 plasma antibody levels sufficient to mediate ADCC and tier 1 neutralization (Rerks-Ngarm et al., 2009). Furthermore, the binding footprints of the isolated V2 mAbs overlap with a tripeptide motif in V2 (position 179–181) that binds the adhesion receptor α4β7 (Arthos et al., 2008). Antibodies that block this interaction have been shown to reduce simian immunodeficiency virus (SIV) acquisition and impact pathogenesis in the non-human primate model (Byrareddy et al., 2014, 2016).

Structural studies of two RV144 mAbs, CH58 and CH59, showed that the V2 peptide epitope can be structurally dynamic, as both mAbs bound to different conformations of V2

(Liao et al., 2013). CH58 recognizes region 167–176 as an α-helix, and 177–181 as coiled loop, while CH59 binds region 168–173 as a coil, and 174–176 as a short 3_{10}-helix. This differs from bNAbs, which only bind conformational epitopes that include region 167–181 as one of five β-strands forming part of a "Greek key motif" in prefusion Env trimers (Gorman et al., 2016; Julien et al., 2013; McLellan etal.,2011; Pancera et al., 2014). Non-neutralizing V2 antibodies previously isolated from HIV-1-infected donors (such as 830A) also bind to this five-stranded β-barrel conformation of V2, but their epitopes are not exposed on native, pre-fusion trimers (Pan et al., 2015). Similarly, the peptide epitopes recognized by vaccine antibodies CH58 and CH59 are likely only present on aberrantly processed or refolded forms of V2, which coexist with native pre-fusion Env on the viral membrane (Moore et al., 2006). These aberrant forms of Env are the primary target for non-neutralizing antibodies mediating Fc effector functions, which may have contributed toward the reduced infection risk in RV144.

In the case of RV144 V2 antibodies, these antiviral activities were largely dependent on the interactions with positively charged residues at positions 168, 169, and 171 in V2. In both CH58 and CH59, this binding was mediated predominantly by a glutamic-aspartic amino acid pair (ED motif) in the antibody CDRL2 (Liao et al., 2013; Wiehe et al., 2014), which is structurally preconfigured in the naive B cell to interact with V2 (Nicely et al., 2015). Recognition of V2 by other RV144 mAbs, as well as mAbs from vaccinated non-human primates, also required the same ED motif, although alternative solutions could potentially be found among other animal models that lack an appropriate ED-motif-encoding genome (Wiehe et al., 2014, 2017). In humans the ED motif is encoded by only two functionally expressed light chain germline genes, IGLV3–10 and IGLV6–57 (Lefranc, 2001). This suggests a limited capacity for eliciting these types of potentially protective antibodies, even though the V2 region is highly immunogenic, and 20%−45% of HIV-1-infected individuals develop V2-specific antibodies (Israel et al., 1997; Kayman et al., 1994).

Therefore, to assess whether other modes of K169 binding existed, we screened HIV-positive plasma samples for K169-dependent, V2 peptide-binding antibodies, and isolated three mAbs that resembled the RV144 vaccine antibody CH58. All mAbs used the same IGHV5–51 heavy chain, but two mAbs used a light chain that lacked an ED motif. A crystal structure of one of these, CAP228-16H, bound to a V2 peptide revealed how a surrogate DDxD motif enabled binding to K169. The identification of this third light chain gene capable of binding V2 broadens the K169-binding repertoire that can respond to RV144 vaccine antigens. Overall, these data contribute toward a better understanding of K169-focused V2 epitopes and the antibodies that target them, which are considered essential for RV144 vaccine efficacy.

RESULTS

Isolation of V2 Peptide-Binding Antibodies from HIV-1 Infection

To identify HIV-infected individuals with RV144-like antibodies, we screened plasma samples from 15 HIV-1 subtype C chronically infected donors for binding to V2 peptides and V1V2 scaffolded proteins (Figure 1A). Hierarchical clustering of reactivity was used to divide the plasmas into three groups: V2 peptide-binding antibodies (clustering with CH58/

CH59), monomeric V1V2-binding antibodies (clustering with PG9) (Walker et al., 2009), and antibodies with limited-to-no monomer reactivity (clustering with CH01) (Bonsignori et al., 2011). One-half of the selected participants developed bNAbs during infection, including two to the V2 region (CAP256 and CAP257) (Gray et al., 2011a; Moore et al., 2011; Wibmer et al., 2013), but we saw no obvious binding patterns to these antigens among those individuals with bNAbs. Almost all plasma samples contained cross-reactive V1V2 antibodies, with binding to the Case A_gp70 protein used in the RV144 correlates analysis being the strongest. However, only two participants (CAP228 and CAP229) developed high-titer, cross-reactive, V2 peptide-binding antibodies similar to CH58 and CH59 from RV144.

Longitudinal analysis revealed that donor CAP228 developed V2 peptide-binding antibodies within 7 weeks of infection that peaked at 36 weeks and remained high thereafter (Figure 1B). A large proportion of this response was dependent on the K169 residue, as binding to a K169E mutant peptide was considerably reduced. CAP228 did not develop neutralization breadth during this time and maintained relatively low viral loads for 6 years before initiating antiretroviral therapy. To find representative mAbs, memory B cells from CAP228 were isolated at 134 and 174 weeks post-infection (wpi) using a differential K169/E169 single-cell sorting strategy (Figure 1C). A total of 416 cells were sorted, yielding three K169-dependent mAbs that bound strongly to V2 peptides in ELISA (Figure 1D). The mAb CAP228–3D was isolated at 134 wpi only, while a related pair of mAbs, CAP228-16H/19F, were isolated at both 134 and 174 wpi. When compared with RV144-elicited antibodies, the CAP228 antibodies were relatively less affected by the K169E substitution, with only a 10-fold reduction in EC_{50} compared to CH58 where binding was knocked out. CH59 failed to bind the CAP45 V2 peptides (not shown). All three CAP228 mAbs shared a common *IGHV5–51* heavy chain gene also used by CH58 (Figure 1E, highlighted in blue). CAP228–3D also used the same *IGLV6–57* gene as CH58, while CAP228-16H and CAP228-19F (which are clonally related) used a *IGLV3–21* light chain gene (Figure 1E, highlighted yellow and purple). This latter gene does not encode the characteristic K169-binding CDRL2 ED motif but does have potentially analogous negatively charged residues at the same positions (Figure 1E, bolded in red). The CAP228-3D antibody had a 19-amino acid-long CDRH3 (as defined by the ImMunoGeneTics database), like CH58, while the CDRH3s of CAP228-16H/19F were slightly shorter (16 amino acids), although still relatively longer than the average CDRH3 lengths observed for CH59-like antibodies (Wiehe et al., 2014). All three CAP228 antibodies had moderately higher levels of mutation as expected for antibodies from infection when compared to those after immunization. Most noticeably, mutation levels of the two IGLV3–21 light chains (antibodies CAP228-16H/19F) were higher than that of the matched heavy chains, suggesting these may have been under stronger selection pressure.

The K169-Dependent V2-Binding Repertoire Is Not Limited to ED-Motif Germline Genes

To trace the ontogeny of the CAP228 antibody lineages, gene-specific antibody transcripts were sequenced from peripheral blood mononuclear cells (PBMCs) at seven time points using the Illumina MiSeq platform. Identity-divergence plots revealed clonally related heavy and light chains as early as 7 wpi (Figures S1A and S1B; Table S1), consistent with ELISA mapping data showing the rapid elicitation of V2-binding antibodies (refer to Figure 1B).

Despite this rapid emergence, the CAP228 V2 antibodies were not autoreactive and were thus unlikely to have arisen from a preexisting polyreactive B cell pool (Table S2). Although CAP228-16H was isolated at 134 wpi, exact matches to the heavy chain of this antibody were detected at 96, 134, and 174 wpi, while CAP228-16H/19F lineage-related reads were detected at all time points sequenced (Figures S1A, S2A, and S2B). In contrast, while CAP228-3D clonally related light chains were found at all time points sampled, related heavy chains were only detected above threshold at 47 wpi (Figures S1B, S3A, and S3B). CAP228-3D uses the same heavy chain V gene as CAP228-16H/19F and was thus amplified using the same IGHV5–51-specific primers, suggesting a sampling bias that might represent increased clonal expansion of this family when compared to the CAP228-3D lineage. Maximum-likelihood phylogenetic trees for the heavy and light chains of the CAP228-16H/19F lineage (and the light chains of the CAP228-3D lineage) were drawn using the isolated antibody sequences and clonally related MiSeq reads to estimate lineage evolution (Figures 2A and S1C). The CAP228-16H/19F unmutated precursor (or UCA) was identified directly from these data using the least mutated common ancestor (LMCA) of clonally related heavy and light chain sequences from 7 wpi, while the CAP228-3D precursor was calculated by germline reversion of the heavy chain, matched with the LMCA light chain from related reads at 7wpi.

The predicted CAP228-16H/19F light chain UCA shared the highest similarity with the IGLV3–21*01 allele, which encodes a tyrosine-aspartic acid pair (YD) at position 49–50 in the CDRL2 rather than the two aspartic acids (DD) observed in the CAP228-16H/19F lineage (Figure 2B, highlighted yellow and blue). However, the CAP228-16H UCA also shared a synonymous allelic similarity with the DD-encoding IGLV3–21*02/03 alleles at position 92 (Figure 2B, highlighted red). To confirm the origin of the CAP228-16H/19F lineage, the germline IGLV3–21 alleles of CAP228 were amplified from genomic DNA and sequenced. This revealed two previously undocumented IGLV3–21 alleles, IGLV3–21*01m and IGLV3– 21*01mm (using a similar nomenclature for novel alleles as previously reported in Scheepers et al., 2015), where IGLV3– 21*01m had a single synonymous mutation at position 92 (also found in IGLV3–21*02/03) when compared to IGLV3– 21*01. IGLV3–21*01mm further differed from IGLV3–21*01m by also including the non-synonymous change from Y to D at position 50 (Figure 2B, bottom row). Both the IGLV3– 21*01m and IGLV3–21*01mm predicted UCA variants were synthesized and tested for their ability to bind the transmitted/founder autologous CAP228 V1V2 in ELISA. Only the DD-encoding UCA (IGLV3–21*01mm) bound the antigen (Figure 2C, blue and yellow lines). Together with longitudinal lineage sequencing, these data suggested that the IGLV3– 21*01mm allele with the CDRL2-encoded DD pair initiated the CAP228-16H/19F lineage.

Since the IGLV3–21*01mm allele has not been previously described, we also assessed the known IGLV3–21*02/03 DD-encoding alleles for their ability to engage V2 antigens. Both the I48V mutation (that reverted the CAP228-16H/19F UCA to IGLV3–21*03) as well as the K17Q mutation (converting the CAP228-16H/19F UCA to IGLV3–21*02) bound equally well to V1V2 (Figure 2C, pink and purple lines), confirming the relevance of both common IGLV3–21 allelic variants in the V2-targeted immune response. An analysis of allelic frequencies using ExaC (Lek et al., 2016) suggested that the average prevalence of DD-encoding IGLV3–21 alleles in the general population is 60% (Figure 2D). The only

population group to show significant variation from this was East Asia, where the frequency was much lower at 26%, perhaps explaining why this light chain was not represented among RV144 mAbs. Overall, the identification of this additional light chain broadens the pool of potential K169-dependent V2-reactive human B cells able to respond to RV144 antigens.

The IGLV3–21 CDRL2 DDxD Motif Interacts with V2 Residues K168, K169, and Y173

As CAP228-16H/19F lacked the CDRL2 ED motif used by vaccine-elicited mAbs to interact with positively charged residues at positions K168 and K169/K171, we hypothesized that the negatively charged DD residues in the IGLV3–21 CDRL2 could make similar contacts with V2. To investigate this, a cocrystal structure of CAP228-16H bound to the heterologous CAP45 V2 peptide (residues 164–182) was determined at 2.6 A resolution (Figure 3; Table 1). CAP228-16H bound to V2 in a conformation that was highly similar to CH58 (Liao et al., 2013), with the N-terminal half of the peptide adopting an a-helical conformation, and the C-terminal portion, a random coil structure (Figure 3A). Electrostatic analysis of the CAP228-16H light chain paratope revealed a large anionic patch, created by three aspartic acid residues in the CDRL2 at positions 50, 51, and 53 (Figure 3B, highlighted in red). This formed a DDxD motif that was analogous to the ED motif of CH58 (positions 50 and 51), but covering a relatively larger surface area.

An aspartic acid at position D51 was common to both antibodies and was similarly oriented to interact with K168 in V2 (Figure 3C, boxed in pale blue). In contrast, the D50 side chain of CAP228-16H is one carbon shorter than the E50 residue of CH58, potentially weakening any interactions with K169. Instead, K169 forms a surrogate water-mediated interaction with the IGLV3–21 germline encoded D53 residue, broadening the K168-K169 recognition motif to include an additional negatively charged side chain (Figure 3C, boxed in pale red). The space vacated by K169 is instead occupied by the CAP45 Y173 residue, which forms a hydrogen bond with D50 that is not seen in the interaction between CH58 and the TH023 V2 peptide, containing the H173 immunotype (Figure 3C, boxed in pale green). To assess the effectiveness of the IGLV3–21 CDRL2 as a surrogate for the IGLV3–10 or IGLV6–57 encoded ED motif, position 50 of the CAP228-16H light chain was mutated to glutamic acid (E) and assessed for binding to the transmitted/founder autologous CAP228 V1V2 in ELISA. The ED version of CAP228-16H bound equally well to V2 when compared with the original DDxD version, with only a twofold difference in EC_{50} (Figure 3D). Altogether, these data confirm the suitability of the DDxD motif to serve as a surrogate for the ED motif, by forming a larger anionic patch that recognizes V2 residues K168 and K169, and also forms interactions with position Y173.

The tyrosines at V2 residues 173 and 177 are also potentially subject to tyrosine sulfation, which is thought to stabilize prefusion trimers through CCR5 mimicry (Cimbro et al., 2014, 2016). Intriguingly, while the V2 peptide used here for structural study was not synthesized with sulfated tyrosines, we observed additional density around position Y177, which we attributed to a sulfate ion that facilitated cocrystallization of the CAP228-16H/V2 complex by also forming important crystal lattice contacts. This sulfate ion was likely from the mother liquor during crystallization but was fortuitously oriented to occupy the same space as a sulfated tyrosine would on virion-associated V1V2 (Figure 3E). An arginine at position

97 in the CAP228-16H CDRH3 interacts directly with the Y177-associated sulfate ion, suggesting that during HIV-1 infection the CAP228-16H lineage could have evolved to recognize a post-translationally sulfated Y177 residue. This ability to bind sulfated tyrosines potentially increases the functional activity of the CAP228 antibodies.

CAP228 Antibodies Mediate ADCC against Globally Prevalent V2 Immunotypes

To compare the epitope of CAP228-16H with the vaccine-elicited antibody CH58, the percentage of accessible surface area for each V2 amino acid side chain that was buried within the respective antibody paratopes was compared in the two crystal structures (Figure 4A). The overall binding profile was strikingly similar, with K168, A/V172, Y/H173, L175, F176, K/R178, and D180 burying more than 50% of their accessible surface area in the antibody paratope and forming major components of the antibody binding sites. These positions are among the most conserved in V2 across globally circulating strains in the Los Alamos National Laboratory HIV-1 Env database and are likely important determinants of the cross-reactivity for V2-binding antibodies (Figure 4B). Several key differences between the two antibodies were also apparent (Figure 4A, highlighted in yellow). Unlike CH58, CAP228-16H did not make strong salt bridges with K169 and K171, both of which are relatively more sequence-variable residues across different strains of HIV-1. CAP228-16H and CH58 both sequester the amino acid side chain at position 173 almost in its entirety but make specific hydrogen bonds with the Y173 or H173 immunotypes, respectively. The Y173 immunotype recognized by CAP228-16H is present in the majority (~65%) of HIV-1 circulating strains (Figure 4B, boxed in yellow), with a higher proportion of H173 found among clade AE viruses (55% when compared to 19% globally), which includes the RV144 vaccine strain. Together with a reduced dependence on sequence-variable residues at positions 169 and 171, and the ability to recognize Y177 sulfation, these data suggest that CAP228-like antibodies might better recognize more globally dominant V2 immunotypes.

To assess whether these recognition differences might impact on the antiviral activities of V2-binding antibodies, the ability of the CAP228 mAbs to mediate both neutralization and ADCC was tested. Similar to CH58 and CH59, the CAP228 antibodies were able to neutralize some tier 1A viruses in a TZM-bl neutralization assay (Figure 4C), but they displayed marginally more activity than CH58 and were able to neutralize both the subtype AE TH023 (neutralized by CH58 and CH59) and the subtype C MW965 strains (the latter with good potency; highlighted in red on the heatmap). However, none of the other tier 1A viruses, including those from subtype C, was sensitive to any of the CAP228 mAbs. For the most part, tier 1A neutralization sensitivity tracked well with the presence of a lysine at position 169 (with the exception of SO032). These mAbs also failed to neutralize tier 1B and tier 2 viruses, including the CAP228 autologous transmitted/founder virus, consistent with the occlusion of these epitopes on entry-competent envelope trimers (Table S3).

The ADCC activity of the CAP228 mAbs was initially assessed by the granzyme B assay using a clade C gp120from strain 1086. All mAbs were re-expressed in an IgG1 backbone containing three alanine mutations in the CH2 domain that improves FcγRIIIA engagement (Ferrari et al., 2011 ; Shields et al., 2001). In this format, all three CAP228 antibodies had ADCC activity comparable to the RV144 vaccine antibodies CH58 and CH59 (Figures 4D

and S4A). The mAb A32 is specific for the inner domain of gp120, has a well-defined ADCC activity, and was used as the positive control (Ferrari et al., 2011; Moore et al., 1994), while Palivizumab (a non-HIV respiratory syncytial virus [RSV]-specific mAb) was used as the negative control. The specificity of the ADCC activity was determined by introducing K169E or H173Y mutations into the 1086 gp120. The K169E mutation substantially affected ADCC by CAP228-16H/19F and almost completely abrogated the activity of CAP228–3D and CH58 (Figure 4D, cyan). In contrast, the H173Y mutation only affected the ADCC activity of CH59, consistent with previous studies (Liao et al., 2013). Control antibodies A32 or Palivizumab remained unaffected by either mutation.

The breadth of ADCC mediated by the CAP228 mAbs was then assessed against the autologous transmitted/founder virus, as well as a multiclade panel of viruses (Figures 4E and S4B), using an infected cell assay where cell killing is measured as a reduction of the Luciferase signal provided by the infected cells (Pollara et al., 2014). The CAP228 mAbs showed broader and more potent reactivity compared to CH58 (Figure 4E, highlighted in red), mediating high levels of ADCC against 6 of the 12 infected cell targets including the CAP228 transmitted/founder virus (Figure 4D, labeled in gray). This difference appeared to track with the immunotype at position 173 (Figure 4D, shaded green or purple). RV144 mAb CH58 only showed high ADCC activity against viruses with an H173 immunotype, mediating weak, sporadic killing of cells infected with the Y173 immunotype, while CH59 was intolerant of the Y173 immunotype. The ADCC potency of all five V2 antibodies also tracked well with changes at position 169, where 169R viruses displaying resistance to all mAbs, while 169T or 169I were resistant to the CAP228 mAbs, or CH58 respectively. For a few viruses, ADCC activity was more moderate/weak and differed between the CAP228 mAb lineages. Both CM244 and TV1.21 have longer, more glycosylated V1 loops compared to the other viruses (32- and 37-amino acid loop lengths and 6 glycans, respectively), potentially contributing to resistance. Overall, these data are consistent with ADCC directed to a V2 epitope and demonstrate the ability of CAP228 mAbs to recognize a broader range of viral immunotypes.

DISCUSSION

The V2 region of the HIV-1 envelope has become an increasingly attractive target for vaccine immunogen design following the demonstration that V2 peptide-binding antibodies correlated with reduced risk of infection in the RV144 vaccine trial (Haynes et al., 2012; Rerks-Ngarm et al., 2009). Recognition of these V2 antigens relies on key interactions with lysine residues at positions 168, 169, and 171 through a mechanism thought to be restricted to two light chain V genes. Here, we identify an additional light chain V gene that uses an alternative mode of recognition, allowing for broader reactivity with global strains. The CAP228 mAbs, isolated from an HIV-1 subtype C-infected individual, were shown to mediate ADCC against a larger panel of infected cells compared to mAbs from RV144. Overall, these data improve our understanding of the immunogenicity of V2 and suggest an increased ability to respond to RV144-like vaccines in populations where suitable alleles are more prevalent.

The isolation of antibodies from HIV-1-infected donors that resemble those from vaccine recipients suggests that RV144 mAbs were elicited by envelope conformations that are naturally expressed during HIV-1 infection. As such, studies of mAbs isolated from donors such as CAP228 are highly relevant for understanding how the RV144 vaccine may have mediated its protective effect. Screening of donor sera revealed that while antibodies to V2 were commonly elicited during chronic HIV-1 infection, only 2 of 15 individuals showed a dominant binding pattern similar to the RV144 mAbs CH58 and CH59. This suggests that cross-reactive, linear peptide-associated, K169-dependent V2 response may be less immunodominant in HIV infection, and perhaps explains why these types of V2 mAbs have not previously been isolated from infected donors. In keeping with this, we found the frequency of V2 K169-specific B cells in CAP228 to be extremely low, as less than 1 per 25,000 memory B cells were isolated by the differential sorting approach.

Transcripts from both CAP228 mAb lineages were detected at 7 wpi, suggesting that they arose early, and possibly simultaneously, co-incident with the appearance of V2-binding antibodies in CAP228 serum. All of the CAP228 mAbs showed subtle differences in V2 recognition compared to CH58, including being considerably less dependent on residue K169, which may reflect their need to adapt to an evolving viral antigen. Of the two lineages, CAP228–3D was most CH58-like in that it shared the same IGLV6–57 light chain gene. However, transcripts from the CAP228–3D lineage were found at very low frequency, with detection of the heavy chain only at a single time point. In contrast, the CAP228-16H/19F lineage heavy and light chain transcripts were seen across all time points, peaking at 47 weeks (which coincided with high V2-binding titers) and appeared to be the dominant response. Whether or not the unique heavy-light chain pairing of the CAP228-16H/19F lineage conferred a selective advantage is still to be determined. Similarly, the isolation of two lineages that used the same heavy chain as CH58 may indicate a genetic advantage for IGHV5–51 when accessing the V2 site that warrants further study.

Antibodies able to bind V2 peptides were thought to be limited to the two germline light chain genes IGLV3–10 and IGLV6–57 that contain a pre-configured ED motif (Wiehe et al., 2014). Similarly, mAbs isolated from V2-immunized rhesus macaques almost always used the IGLV3–17 light chain gene (an ortholog of human IGLV3–10) (Wiehe et al., 2014). This suggested a potential genetic restriction within the naive repertoire of B cells able to respond appropriately to RV144-type vaccines. Our identification of an additional light chain gene used by CAP228-16H/19F, which can form productive K169-dependent V2 peptide interactions, is therefore encouraging. Structural studies revealed that this IGLV3–21 light chain uses a different CDRL2 arrangement to bind K169, which allowed us to define a DDxD motif that serves as a surrogate for the ED motif. Generation of an artificial antibody with an EDxD motif revealed equivalent binding activity, indicating that this allele can accommodate the traditional mode of binding, although the precise interactions would need to be confirmed structurally. Two of the International Immunogenetics Database (IMGT)-defined IGLV3–21 alleles (*02 and *03) have this DDxD motif, while the third IGLV3–21*01 allele has a YDxD motif. Interestingly, germline sequencing of IGLV3–21 from donor CAP228 revealed two alleles not previously reported in the IMGT database (Lefranc, 2001), indicating the importance of more inclusive online databases. Expression and testing of the UCA with a YDxD motif (IGLV3–21*01m) suggested that B cells carrying this allele

were not engaged by the infecting virus. Rather, this lineage derived from the IGLV3–21*01mm allele, containing the DDxD motif. Reversion of IGLV3–21*01mm allele to contain the *02 and *03 amino acid changes showed no impact on binding to the autologous CAP228 transmitted/founder V1V2, suggesting that all DDxD-motif-containing alleles are equally functional in binding V2 antigens. The discovery of two undocumented alleles in one individual, in addition to the three previously reported alleles within the IGLV3–21 light chain gene, suggests that significant variation exists within the African genome as previously demonstrated for the heavy chain variable region (Scheepers et al., 2015). Since the IGLV3–21*01mm allele contains the DDxD motif, this increases the repertoire of light chain alleles able to bind V2 and could increase V2 antibody response rates and titers to RV144-like vaccines.

In addition to expanding the B cell repertoire able to recognize K169, the IGLV3–21 gene used by CAP228-16H also forms productive interactions with Y173 in V2, potentially conferring increased recognition of heterologous strains. Consistent with this, CH58 showed strong ADCC against viruses with the H173 immunotype, while CAP228 antibodies recognized viruses that contained both the H173 as well as the more globally prevalent Y173 immunotype. These data suggest that the ability to accommodate Y173, in part due to the use of this newly implicated IGLV3–21 light chain, may have resulted in broader ADCC activity, and these results are consistent with the relatively high ADCC activity previously measured in CAP228 plasma (Richardson et al., 2018). Antibodies from RV144, such as CH58, were elicited by a vaccine strain with an H173 immunotype that is relevant to clade AE (which predominates in Thailand), while CAP228 antibodies were elicited by a virus with a Y173 immunotype. While this likely contributed to selection of IGLV3–21 used by the CAP228-16H/19F mAbs, the CAP228–3D mAb (which uses an ED-motif-containing light chain) was also elicited by the same Y173-containing viruses. CAP228–3D interactions with Y173, like CH58 interactions with H173, are exclusively mediated by the heavy chain CDRH3. Another RV144 mAb, CH59, binds to a different H173-dependent conformation of V2 but failed to bind the peptides or V1V2 scaffolded proteins used in this study with the more globally prevalent Y173 immunotype. The specific immunotype presented at position 173 might therefore form an important antigenic determinant of V2 immunogens. Similarly, the ability to recognize a sulfated Y177 residue, which is less frequently observed on recombinant immunogens when compared with virus associated V1V2 (Cimbro et al., 2014), may improve V2 mAb antiviral activities. These data highlight key differences between CAP228 antibodies elicited through HIV-1 infection, which were more cross-reactive with circulating viral strains than mAbs elicited by vaccination, and suggest that antigens more representative of the diversity within V2 could elicit broader and more potent antiviral responses than RV144.

ADCC activity was identified as a correlate of reduced risk of HIV-1 infection, and mAbs isolated from RV144 also showed strong ADCC activity (Bonsignori et al., 2012; Haynes et al., 2012; Pollara et al., 2014). Here, we show that the ADCC activity of all tested V2 mAbs was largely restricted to cells infected with viruses that harbored a K169 residue in V2, although the IGHV5– 51/IGLV3–21 pairing appeared to be more tolerant of variation at this position. This further supports the genetic signature analysis showing that breakthrough infections in RV144 were under-represented for K169 (Rolland et al., 2012). While this has

been attributed to a genetic sieve effect, i.e., that K169-containing viruses were selectively prevented from establishing infection, mutations away from K169 may also have arisen post-acquisition as a result of antibody selection pressure, possibly through ADCC (Rolland et al., 2012). Increasingly, the Fc effector functions of antibodies have been shown to play an important role in antiviral efficacy (Horwitz et al., 2017), but direct evidence for viral selection is limited mainly because of the difficulty of analyzing the role of ADCC separately from that of antibody neutralizing activities.

The RV144 trial conducted in Thailand is the only HIV-1 vaccine to show some level of efficacy, and follow-up studies of this approach are being actively pursued. In the HVTN 097 phase I trial, which tested the same vaccines used in RV144, antibody responses to V2 were found to be higher in Africans compared to Thais (Gray et al., 2014). A follow-up study called HVTN 100, that used clade C versions of these vaccine immunogens, passed all pre-set go/no-go criteria, which included V2 antibody response rates (Bekker et al., 2018). These data suggest that V2 antibodies will be readily elicited in HVTN 702, the current efficacy study that is enrolling 5,400 high-risk men and women in South Africa. It remains to be seen whether modifications to the regimen, which includes new HIV-1 clade C components, additional protein boosting, and a different adjuvant, results in higher levels of efficacy compared to RV144. Importantly, this trial will confirm whether or not V2 antibodies with ADCC activity are a correlate of reduced risk of HIV-1 infection. Our data, showing that South Africans can respond to V2 antigens using additional genetic determinants, expands the opportunities for responding favorably to RV144-like vaccines, but confirmation of this awaits isolation and characterization of mAbs from participants in the HVTN 702 trial.

STAR★METHODS

CONTACT FOR REAGENT AND RESOURCE SHARING

Further information and requests for resources and reagents should be directed to and will be fulfilled by the Lead Contact, Prof. Lynn Morris (lynnm@nicd.ac.za).

EXPERIMENTAL MODEL AND SUBJECT DETAILS

CAPRISA cohort—The CAPRISA 002 Acute Infection study, established in 2004, followed HIV-1 subtype C infected adult women (>18 years) attending urban and rural clinics from seroconversion through to the initiation of antiretroviral therapy in Durban and Vulindlela, South Africa (van Loggerenberg et al., 2008). It was reviewed and approved by the research ethics committees of the University of KwaZulu-Natal (E013/04), the University of Cape Town (025/2004), and the University of the Witwatersrand (MM040202). All participants provided written informed consent for study participation. CAP228 enrolled into this study following infection with a HIV-1 subtype C virus in March 2005. She was initially identified as a virological controller, having a CD4 count of > 350 cells/mL and a viral load of < 2000 copies/mL on at least two consecutive measurements after 6 months of infection (Gray et al., 2007). However, antiretroviral therapy was started in June 2012 following a peak viral load of 228,207 RNA copies/mL at 370 wpi.

METHOD DETAILS

Cell sorting—Single-cell sorting of antigen-specific B cells was performed as previously described (Morris et al., 2011; Wu et al., 2010) with the following modifications. Biotinylated CAP45 cyclic peptides comprising gp120 residues 157 – 196 (Genscript) were labeled with either Brilliant Violet 421 (BV421, Biolegend), or AlexaFluor 647 (AF647, Life Technologies), conjugated to streptavidin. CAP228 PBMCs were stained with a variety of cell surface markers (BD Biosciences) as well as live/dead stain (Invitrogen), and antigen-specific memory B cells were sorted as CD3-, CD14-, CD16-, CD19+, IgD- and CAP45 peptide K169+ E169- into 96-well PCR plates containing lysis buffer, using a BD FACS Aria II (BD Biosciences). In a second sort, the CAP228 autologous transmitted/founder V1V2 domain was scaffolded onto PDB ID: 1FD6 (McLellan et al., 2011), and labeled with BV421 as an addifigtional positive bait. Data were analyzed using FlowJo (Tree Star).

Single cell PCR amplification of heavy and light chain variable genes—The genes encoding IGHV and IGLV chains were amplified from sorted cells by RT and nested PCR using a combination of two published methods. Reverse transcription was performed using Superscript III reverse transcriptase (Invitrogen) and random hexamer primers. Following cDNA synthesis VH, Vκ, and Vλ antibody genes were amplified as previously described (Doria-Rose et al., 2015; Liao et al., 2009). Primer sequences are listed in Tables S4 and S5.

Protein expression and purification—Sorted mAbs were first amplified as linear cassettes used directly to transfect HEK293T cells (obtained from the NIH AIDS Research and Reference Reagent Program, Division of AIDS, NIAID, NIH) grown at 37°C, 10% CO_2. The resulting supernatants were tested in ELISA for IgG concentration and antigen reactivity as previously described (Gray et al., 2011b). Following confirmation of expression and binding, the mAbs were sub-cloned and expressed in a wild-type IgG1 backbone, as well as an IgG1 backbone with the S298A, E333A, and K334A mutations in CH2 (3A variant) for ADCC experiments (Shields et al., 2001). Monoclonal antibodies were produced by co-transfection of heavy and light chain encoding plasmids into HEK293F cells (Invitrogen) grown at 37°C, 5% CO_2, 70% humidity, and 125 rpm. Cultures were harvested after seven days by centrifugation at 3000 xG, and supernatants were filtered through 0.22 mm before purification by protein A chromatography.

V1V2 scaffolded miniproteins were expressed in HEK293S cells grown at 37°C, 5% CO_2, 70% humidity, 125 rpm (ATCC CRL-3022, N-acetylglucosaminyltransferase I deleted), to yield a uniform low-mannose glycan content. Cultures were harvested after seven days as above and purified by sequential Ni-NTA and size exclusion (SEC) chromatography.

ELISA

Biotinylated cyclic V2 peptides from CAP45 (JPT peptides) were captured onto Streptavidin coated ELISA plates at a concentration of 2 ng/mL at 37°C for one hour. Plates were blocked with 5% milk and washed in PBS (0.05% tween$_{20}$) before being probed at 37°C for one hour with serial dilutions of sample antibodies, starting at 10 mg/mL. After a subsequent washing step, HRP-conjugated goat anti-human IgG (H+L) polyclonal antibodies (Sigma-

Aldrich) diluted to 1:5,000 were added to the plate and incubated for one hour at 37°C. Bound antibodies were detected using TMB substrate, and the reactions were stopped by the addition of 1 M H_2SO_4. Absorbance was read at 450 nm.

The CAP228 V1V2–1FD6 scaffolds were coated at 5 mg/mL onto high protein-binding microplates overnight at 4°C. Plates were blocked and washed as above, and probed with plasma serially diluted from 1:100, or mAbs from 10 mg/mL, for one hour at 37°C. Following washing, bound antibodies were detected with HRP-conjugated anti-human antibodies (Sigma-Aldrich) at a concentration of 1:1000 for one hour at 37°C, followed by TMB substrate stopped with 1 M H_2S0_4. Absorbance was read at 450 nm.

Neutralization assay—Single round of replication Env-pseudotyped viruses were prepared using the pSG3DEnv plasmid in HEK293T cells, and titered to infect TZM-bl target cells as described previously (Montefiori, 2009). Cell lines and virus plasmids were obtained from the NIH AIDS Research and Reference Reagent Program, Division of AIDS, NIAID, NIH. Neutralization was calculated as a reduction in luminescence units compared with control wells, and reported as 50% inhibitory concentration (IC_{50}).

Infectious molecular clones (IMC)—The HIV-1 reporter virus used was a replication-competent infectious molecular clone (IMC) designed to encode the 1086.B2 (subtype C; GenBank No. FJ444395), CM235.2 (subtype A/E; GenBank No. AF259954.1), CM244 (subtype A/E; GenBank No. KC822429), CAP228.2.00.51J (subtype C; GenBank No. EF203968), MW965.26 (subtype C; GenBank No.U08455), DU151.2 (subtype C; GenBank No. DQ411851), TV1.21 (subtype C; GenBank No. HM215437), C1080.3 (subtype AE; GenBank No. JN944660), WITO.c (subtype B; GenBank No. JN944948), CH040.c (subtype B; GenBank No. JN944939), Q23.17 (subtype A; GenBank No. AF004885) and CH0505.w4.24 (subtype C; GenBank No. KC247577) *env* genes in *cis* within an isogenic backbone that also expresses the *Renilla* luciferase reporter gene, and preserves all viral open reading frames (Edmonds et al., 2010; Li et al., 2005). The subtype AE Env-IMC-LucR virus used was the NL-LucR.T2A-AE.CM235-ecto (IMC_{cM235}) (plasmid provided by Dr. Jerome Kim, US Military HIV Research Program). All the other IMCs were built using the NL-LucR.T2A-ENV.ecto backbone as originally described (Adachi et al., 1986). Reporter virus stocks were generated by transfection of HEK293T cells with proviral IMC plasmid DNA, and titered in TZM-bl cells for quality control.

Coated ADCC assay—ADCC activity was detected by the previously described ADCC-GranToxiLux (GTL) assay using antigen-coated cells (Pollara et al., 2011). Whole PBMCs from a healthy donor were used as effector cells for which the FcgRIIIa receptor was genotyped as being homozygous for valine at position 158 by the TaqMan SNP genotyping assay (rs396991) (Applied Biosystems) to ensure high levels of lysis. Target CEM-NKR.CCR5 cells were coated with wild-type 1086 gp120 and K169E or H173Y mutants at optimal concentrations determined by titration. The monoclonal antibody A32 was used as a positive control and Palivizumab (MedImmune, LLC) was used as the negative control. The results were analyzed in FlowJo (FlowJo LLC) and are shown as % Granzyme B (GzB) activity, defined as the percentage of cells positive for proteolytically active GzB out of the total viable target cell population. The final results exclude the subtracted background value

determined by the % GzB activity observed in wells containing effector and target cell populations in the absence of IgG.

Infected cell ADCC assay—The infected cell assay was used to measure ADCC activity as previously described (Pollara et al., 2014). We utilized a modified version of our previously published ADCC luciferase procedure (Karasavvas et al., 2012; Liao et al., 2013). Briefly, a laboratory-derived clone of the CEM.NKR$_{ccR5}$ cell line (NIH AIDS Reagent Program, Division of AIDS, NIAID, NIH from Dr. Alexandra Trkola) was used as targets for ADCC luciferase assays after infection with the HIV-1 IMCs listed above (Trkola et al., 1999). The target cell line was infected with IMC using titered stock that generated more than 20% infected target cells after 48–72 hours of infection. The target cells were incubated with 5-fold serially diluted mAbs starting at 50 mg/mL. Cryopreserved peripheral blood mononuclear cells (PBMC) obtained from an HIV-1 seronegative donor with the geographically common 158F/V Fcg receptor IIIa phenotype were used as source of effector cells. After thawing, the cryopreserved PBMCs were rested overnight and used at an effector to target ratio of 30:1. The effector cells, target cells, and Ab dilutions were plated in opaque 96-well half area plates and incubated for 6 hours at 37°C in 5% CO_2. The final readout was the luminescence intensity (in relative light units) generated by the presence of residual intact target cells, that have not been lysed by the effector population in the presence of any ADCC-mediating mAb. The percentage of killing was calculated using the formula:

$$\% \ killing = \frac{(RLU \ of \ Target \ and \ Effector \ well) - (RLU \ of \ test \ well)}{RLU \ of \ Target \ and \ Effector \ well} \times 100$$

In this analysis, the RLU of the target plus effector wells represents spontaneous lysis in absence of any source of antibody. The RSV-specific mAb Palivizumab was used as a negative control and A32 as the positive control. Data are represented as the area under the curve of percentage specific killing over the serially diluted antibodies, calculated above a 15% background cutoff.

Autoreactivity assays—All isolated mAbs were screened for autoreactivity using the ZEUS AtheNA Multi-Lyte® ANA-II Plus Test System (Zeus Scientific), which semiquantitatively detects IgG antibodies to 8 separate analytes: SSA, SSB, Sm, RNP, Scl-70, Jo-1, Centromere B, and Histone as previously described (Haynes et al., 2005).

Next generation sequencing using the Illumina MiSeq platform—Total RNA was extracted from cryopreserved PBMC using the QIAGEN AllPrep DNA/RNA mini kit as per the manufacturer's specifications, and reverse transcription was carried out using Random Hexamers and Superscript III RT enzyme (Thermo Fisher Scientific). Primers specific to the heavy and light chains (Tables S4 and S5) of CAP228-16H and CAP228–3D were based on previously published primers (DeKosky et al., 2013; Doria-Rose et al., 2014; Liao et al., 2009), such that forward primers binding in the leader sequence orV-region (VH5int, VL3–21, and VL6–57) and reverse primers in the constant region (IGHG R, 3CL) were modified for use on the Illumina MiSeq Platform. Samples from each time point were amplified seven times for both the heavy and light chains to ensure adequate coverage and minimize PCR bias. A plasmid control containing the CH58 antibody sequence was also amplified. PCR

conditions were as previously described (Scheepers et al., 2015) except that annealing temperatures were 58°C and 55°C for heavy and light chains respectively. Nextera XT Indexing tags were added to the pooled MiSeq amplicon libraries. All products were checked on an Agilent bioanalyser and cleaned-up using 0.75x Ampure Beads (Beckman-Coulter), using the manufacturer's protocol. A final concentration of 12 pM denatured DNA library with 15% PhiX control was run onto the Illumina MiSeq, using the MiSeq reagent kit (version 3) with 2×300 paired-end reads.

Next generation sequencing data processing and analysis—Paired-end MiSeq reads were merged into full-length reads for each time point using PEAR (Zhang et al., 2014). Paired sequences were then de-replicated using USEARCH (Edgar, 2010) resulting in unique reads. The SONAR bioinformatics pipeline (Schramm et al., 2016) was used to identify clonally related reads to CAP228-16H and CAP228–3D. In brief, germline V and J genes were assigned, the CDR3 regions were identified, and identity to CAP228-16H / CAP228–3D for each of the reads was calculated. Identity-divergence plots, created through SONAR, were used to visualize the level of germline divergence from the relevant germline genes and the percentage identity to each antibody for all unique reads. Clonally related sequences were selected based on germline gene usage and CDR3 identity > 80% to the mAbs. To account for sequencing and/or PCR error, all singletons were removed and the remaining sequences were clustered at 99% identity using USEARCH, then one representative was selected from clusters with three or more transcripts for downstream analyses. Best fit models for amino acid maximum likelihood phylogenetic trees were calculated and constructed using MEGA6 and PhyML 3.0 (Guindon et al., 2010; Tamura et al., 2013). The trees were displayed in Dendroscope (Huson and Scornavacca, 2012).

Germline gene amplification and cloning—Primers specific to the IGLV3–21 germline gene were designed (Tables S4 and S5) to amplify all alleles from stored genomic DNA using the HotStarTaq Plus DNA polymerase (QIAGEN), as per manufacture recommendations (with an annealing temperature of 56°C). Amplicons were cloned using the TOPO TA Cloning kit (Thermo Fischer Scientific), then colonies were screened by PCR using TOPO TA kit provided primers, and assessed by Sanger sequencing.

X-ray protein crystallography—The CAP228-16H variable domain was subcloned into an IgG1 expression construct containing a human rhinovirus (HRV) 3C protease cleavage site between the antigen binding (Fab) and crystallizable (Fc) antibody fragments. Expressed full length antibody was digested with HRV 3C (Novagen), and the Fab fragment was purified by negative selection with protein A, before being complexed with V2 peptide (residues 164 – 182) at two-fold molar excess, and further purified by size exclusion chromatography. Fab-peptide complexes were flash frozen at 13.1 mg/mL. The initial crystallization hit (20% polyethylene glycol 8000 (PEG8000), 200 mM sodium chloride, 100 mM $Na_2PO4/C_6H_8O_7$ pH4.2) was identified from a manual 384 well sitting drop screen that included Wizard Precipitant Synergy and Wizard Classic 1–4 screen reagents (Rigaku) mixed at ~1:1 with protein to a total of 400 nL - 600 nL per drop. Crystal growth conditions were further optimized in 15-well hanging-drop vapor diffusion plates (QIAGEN) by successive additive screens to include 160 mM ammonium sulfate and 8% 2-methyl-2,4-

pentanediol (MPD). Crystals grew to approximately 0.3 mm in diameter and were further dehydrated and cryoprotected in a drop containing 25% PEG8000, 250 mM NaCl, 200 mM ammonium sulfate, 100 mM $Na_2PO4/C_6H_8O_7$ (pH4.2), and 25% MPD before flash freezing. The final product was manually thawed briefly 'on-loop' to encourage crystal repacking, and then diffracted to 2.6A at the Brazilian Synchrotron Light Laboratory (LNLS) MX-2 beamline using a 1.00A wavelength at 100K. The data were processed using HKL2000, solved with Phaser using PDB accession no. 4HQQ as the search model, and refined with the PHENIX suite. Models were built in Wincoot using 5% of reflections as an R_{free} test set, and including hydrogen atoms to help avoid clashes. All protein structure images were made with the PyMOL Molecular Graphics System, Version 1.3r1edu (Schrodinger LLC). The structure has been deposited in the PDB with accession code 6FY0.

DATA AND SOFTWARE AVAILABILITY

All flow cytometry data were analyzed using FlowJo (Tree Star). MiSeq reads were merged with PEAR (Zhang et al., 2014), de-replicated and clustered with USEARCH (Edgar, 2010), and processed with the SONAR bioinformatics pipeline (Schramm et al., 2016). Phylogenetic associations were made using MEGA (Tamura et al., 2013) and PhyML (Guindon et al., 2010). The isolated antibody variable domain gene sequences were deposited in GenBank (Accession codes MK119167 to MK119171), and all antibody lineage sequencing data was deposited in the Sequence Read Archive (PRJNA498753 Accession codes: SAMN10334092 to SAMN10334110). Structural data was processed with HKL2000, and subsequently solved and refined with the PHENIX core suite and Wincoot. Structure factors were deposited in the Protein Databank (PDB 6FY0). Graphics were generated using PyMOL (Schrodinger LLC).

Supplementary Material

Refer to Web version on PubMed Central for supplementary material.

ACKNOWLEDGMENTS

REFERENCES

Adachi A, Gendelman HE, Koenig S, Folks T, Willey R, Rabson A, and Martin MA (1986). Production of acquired immunodeficiency syndrome-associated retrovirus in human and nonhuman cells transfected with an infectious molecular clone. J. Virol 59, 284–291. [PubMed: 3016298]

Adams PD, Afonine PV, Bunkoczi G, Chen VB, Davis IW, Echols N, Headd JJ, Hung LW, Kapral GJ, Gross-Kunstleve RW, et al. (2010). PHENIX: a comprehensive Python-based system for macromolecular structure solution. Acta. Crystallogr. D. Biol. Crystallog 66, 486–501.

Arthos J, Cicala C, Martinelli E, Macleod K, Van Ryk D, Wei D, Xiao Z, Veenstra TD, Conrad TP, Lempicki RA, et al. (2008). HIV-1 envelope protein binds to and signals through integrin a4β7, the gut mucosal homing receptor for peripheral T cells. Nat. Immunol 9, 301–309. [PubMed: 18264102]

Auton A, Brooks LD, Durbin RM, Garrison EP, Kang HM, Korbel JO, Marchini JL, McCarthy S, McVean GA, and Abecasis GR; 1000 Genomes Project Consortium (2015). A global reference for human genetic variation. Nature 526, 68–74. [PubMed: 26432245]

Bekker LG, Moodie Z, Grunenberg N, Laher F, Tomaras GD, Cohen KW, Allen M, Malahleha M, Mngadi K, Daniels B, et al.; HVTN 100 Protocol Team (2018). Subtype C ALVAC-HIV and bivalent subtype C gp120/MF59 HIV-1 vaccine in low-risk, HIV-uninfected, South African adults: a phase 1/2 trial. Lancet HIV 5, e366–e378. [PubMed: 29898870]

Bonsignori M, Hwang KK, Chen X, Tsao CY, Morris L, Gray E, Marshall DJ, Crump JA, Kapiga SH, Sam NE, et al. (2011). Analysis of a clonal lineage of HIV-1 envelope V2/V3 conformational epitope-specific broadly neutralizing antibodies and their inferred unmutated common ancestors. J. Virol 85, 9998–10009. [PubMed: 21795340]

Bonsignori M, Pollara J, Moody MA, Alpert MD, Chen X, Hwang KK, Gilbert PB, Huang Y, Gurley TC, Kozink DM, et al. (2012). Antibody-dependent cellular cytotoxicity-mediating antibodies from an HIV-1 vaccine efficacy trial target multiple epitopes and preferentially use the VH1 gene family. J. Virol 86,11521–11532. [PubMed: 22896626]

Buchacher A, Predl R, Strutzenberger K, Steinfellner W, Trkola A, Purtscher M, Gruber G, Tauer C, Steindl F, Jungbauer A, et al. (1994). Generation of human monoclonal antibodies against HIV-1 proteins; electrofusion and Epstein-Barr virus transformation for peripheral blood lymphocyte immortalization. AIDS Res. Hum. Retroviruses 10, 359–369. [PubMed: 7520721]

Byrareddy SN, Kallam B, Arthos J, Cicala C, Nawaz F, Hiatt J, Kersh EN, McNicholl JM, Hanson D, Reimann KA, et al. (2014). Targeting a4β7 integrin reduces mucosal transmission of simian immunodeficiency virus and protects gut-associated lymphoid tissue from infection. Nat. Med 20, 1397–1400. [PubMed: 25419708]

Byrareddy SN, Arthos J, Cicala C, Villinger F, Ortiz KT, Little D, Sidell N, Kane MA, Yu J, Jones JW, et al. (2016). Sustained virologic control in SIV$^+$ macaques after antiretroviral and α4β7 antibody therapy. Science 354, 197–202. [PubMed: 27738167]

Cimbro R, Gallant TR, Dolan MA, Guzzo C, Zhang P, Lin Y, Miao H, Van Ryk D, Arthos J, Gorshkova I, et al. (2014). Tyrosine sulfation in the second variable loop (V2) of HIV-1 gp120 stabilizes V2–V3 interaction and modulates neutralization sensitivity. Proc. Natl. Acad. Sci. USA 111, 3152–3157. [PubMed: 24569807]

Cimbro R, Peterson FC, Liu Q, Guzzo C, Zhang P, Miao H, Van Ryk D, Ambroggio X, Hurt DE, De Gioia L, et al. (2016). Tyrosine-sulfated V2 peptides inhibit HIV-1 infection via coreceptor mimicry. EBioMedicine 10, 45–54. [PubMed: 27389109]

DeKosky BJ, Ippolito GC, Deschner RP, Lavinder JJ, Wine Y, Rawlings BM, Varadarajan N, Giesecke C, Dorner T, Andrews SF, et al. (2013). High-throughput sequencing of the paired human immunoglobulin heavy and light chain repertoire. Nat. Biotechnol 31, 166–169. [PubMed: 23334449]

Doria-Rose NA, Schramm CA, Gorman J, Moore PL, Bhiman JN, DeKosky BJ, Ernandes MJ, Georgiev IS, Kim HJ, Pancera M, et al.; NISC Comparative Sequencing Program (2014). Developmental pathway for potent V1V2-directed HIV-neutralizing antibodies. Nature 509, 55–62. [PubMed: 24590074]

Doria-Rose NA, Bhiman JN, Roark RS, Schramm CA, Gorman J, Chuang GY, Pancera M, Cale EM, Ernandes MJ, Louder MK, et al. (2015). New member of the V1V2-directed CAP256-VRC26

lineage that shows increased breadth and exceptional potency. J. Virol 90, 76–91. [PubMed: 26468542]

Edgar RC (2010). Search and clustering orders of magnitude faster than BLAST. Bioinformatics 26, 2460–2461. [PubMed: 20709691]

Edmonds TG, Ding H, Yuan X, Wei Q, Smith KS, Conway JA, Wiec-zorek L, Brown B, Polonis V, West JT, et al. (2010). Replication competent molecular clones of HIV-1 expressing Renilla luciferase facilitate the analysis of antibody inhibition in PBMC. Virology 408, 1–13. [PubMed: 20863545]

Emsley P, Lohkamp B, Scott WG, and Cowtan K (2010). Features and development of Coot. Acta. Crystallogr. D. Biol. Crystallogr 66, 486–501. [PubMed: 20383002]

Ferrari G, Pollara J, Kozink D, Harms T, Drinker M, Freel S, Moody MA, Alam SM, Tomaras GD, Ochsenbauer C, et al. (2011). An HIV-1 gp120 envelope human monoclonal antibody that recognizes a C1 conformational epitope mediates potent antibody-dependent cellular cytotoxicity (ADCC) activity and defines a common ADCC epitope in human HIV-1 serum. J. Virol 85, 7029–7036. [PubMed: 21543485]

Gorman J, Soto C, Yang MM, Davenport TM, Guttman M, Bailer RT, Chambers M, Chuang GY, DeKosky BJ, Doria-Rose NA, et al.; NISC Comparative Sequencing Program (2016). Structures of HIV-1 Env V1V2 with broadly neutralizing antibodies reveal commonalities that enable vaccine design. Nat. Struct. Mol. Biol 23, 81–90. [PubMed: 26689967]

Gray ES, Moore PL, Choge IA, Decker JM, Bibollet-Ruche F, Li H, Leseka N, Treurnicht F, Mlisana K, Shaw GM, et al.; CAPRISA002 Study Team (2007). Neutralizing antibody responses in acute human immunodeficiency virus type 1 subtype C infection. J. Virol 81, 6187–6196. [PubMed: 17409164]

Gray ES, Madiga MC, Hermanus T, Moore PL, Wibmer CK, Tumba NL, Werner L, Mlisana K, Sibeko S, Williamson C, et al.; CAPRISA002 Study Team (2011a). The neutralization breadth of HIV-1 develops incrementally over four years and is associated with CD4$^+$ T cell decline and high viral load during acute infection. J. Virol 85, 4828–4840. [PubMed: 21389135]

Gray ES, Moody MA, Wibmer CK, Chen X, Marshall D, Amos J, Moore PL, Foulger A, Yu JS, Lambson B, et al. (2011b). Isolation of a monoclonal antibody that targets the alpha-2 helix of gp120 and represents the initial autologous neutralizing-antibody response in an HIV-1 subtype C-infected individual. J. Virol 85, 7719–7729. [PubMed: 21613396]

Gray GE, Andersen-Nissen E, Grunenberg N, Huang Y, Roux S, Laher F, Innes C, Gu N, DiazGranados C, Phogat S, et al. (2014). HVTN 097: Evaluation of the RV144 Vaccine Regimen in HIV Uninfected South African Adults. AIDS Res. Hum. Retroviruses 30, A33–A34.

Guindon S, Dufayard JF, Lefort V, Anisimova M, Hordijk W, and Gascuel O (2010). New algorithms and methods to estimate maximum-likelihood phylogenies: assessing the performance of PhyML 3.0. Syst. Biol 59, 307–321. [PubMed: 20525638]

Haynes BF, Fleming J, St Clair EW, Katinger H, Stiegler G, Kunert R, Robinson J, Scearce RM, Plonk K, Staats HF, et al. (2005). Cardiolipin polyspecific autoreactivity in two broadly neutralizing HIV-1 antibodies. Science 308, 1906–1908. [PubMed: 15860590]

Haynes BF, Gilbert PB, McElrath MJ, Zolla-Pazner S, Tomaras GD, Alam SM, Evans DT, Montefiori DC, Karnasuta C, Sutthent R, et al. (2012). Immune-correlates analysis of an HIV-1 vaccine efficacy trial. N. Engl. J. Med 366, 1275–1286. [PubMed: 22475592]

Horwitz JA, Bar-On Y, Lu CL, Fera D, Lockhart AAK, Lorenzi JCC, Nogueira L, Golijanin J, Scheid JF, Seaman MS, et al. (2017). Non-neutralizing antibodies alter the course of HIV-1 infection in vivo. Cell 170, 637–648.e10. [PubMed: 28757252]

Huson DH, and Scornavacca C (2012). Dendroscope 3: an interactive tool for rooted phylogenetic trees and networks. Syst. Biol 61, 1061–1067. [PubMed: 22780991]

Israel ZR, Gorny MK, Palmer C, McKeating JA, and Zolla-Pazner S (1997). Prevalence of a V2 epitope in clade B primary isolates and its recognition by sera from HIV-1-infected individuals. AIDS 11, 128–130. [PubMed: 9110092]

Julien JP, Cupo A, Sok D, Stanfield RL, Lyumkis D, Deller MC, Klasse PJ, Burton DR, Sanders RW, Moore JP, et al. (2013). Crystal structure of a soluble cleaved HIV-1 envelope trimer. Science 342,1477–1483. [PubMed: 24179159]

Karasavvas N, Billings E, Rao M, Williams C, Zolla-Pazner S, Bailer RT, Koup RA, Madnote S, Arworn D, Shen X, et al.; MOPH TAVEG Collaboration (2012). The Thai Phase III HIV Type 1 Vaccine trial (RV144) regimen induces antibodies that target conserved regions within the V2 loop of gp120. AIDS Res. Hum. Retroviruses 28, 1444–1457. [PubMed: 23035746]

Kayman SC, Wu Z, Revesz K, Chen H, Kopelman R, and Pinter A (1994). Presentation of native epitopes in the V1/V2 and V3 regions of human immunodeficiency virus type 1 gp120 by fusion glycoproteins containing isolated gp120 domains. J. Virol 68, 400–410. [PubMed: 7504740]

Lefranc MP (2001). IMGT, the international ImMunoGeneTics database. Nucleic Acids Res. 29, 207–209. [PubMed: 11125093]

Lek M, Karczewski KJ, Minikel EV, Samocha KE, Banks E, Fennell T, O'Donnell-Luria AH, Ware JS, Hill AJ, Cummings BB, et al.; Exome Aggregation Consortium (2016). Analysis of protein-coding genetic variation in 60,706 humans. Nature 536, 285–291. [PubMed: 27535533]

Li M, Gao F, Mascola JR, Stamatatos L, Polonis VR, Koutsoukos M, Voss G, Goepfert P, Gilbert P, Greene KM, et al. (2005). Human immunodeficiency virus type 1 env clones from acute and early subtype B infections for standardized assessments of vaccine-elicited neutralizing antibodies. J. Virol 79, 10108–10125. [PubMed: 16051804]

Liao HX, Levesque MC, Nagel A, Dixon A, Zhang R, Walter E, Parks R, Whitesides J, Marshall DJ, Hwang KK, et al. (2009). High-throughput isolation of immunoglobulin genes from single human B cells and expression as monoclonal antibodies. J. Virol. Methods 158, 171–179. [PubMed: 19428587]

Liao HX, Bonsignori M, Alam SM, McLellan JS, Tomaras GD, Moody MA, Kozink DM, Hwang KK, Chen X, Tsao CY, et al. (2013). Vaccine induction of antibodies against a structurally heterogeneous site of immune pressure within HIV-1 envelope protein variable regions 1 and 2. Immunity 38, 176–186. [PubMed: 23313589]

McLellan JS, Pancera M, Carrico C, Gorman J, Julien JP, Khayat R, Louder R, Pejchal R, Sastry M, Dai K, et al. (2011). Structure of HIV-1 gp120 V1/V2 domain with broadly neutralizing antibody PG9. Nature 480, 336–343. [PubMed: 22113616]

Montefiori DC (2009). Measuring HIV neutralization in a luciferase reporter gene assay. Methods Mol. Biol 485, 395–405. [PubMed: 19020839]

Moore JP, McCutchan FE, Poon SW, Mascola J, Liu J, Cao Y, and Ho DD (1994). Exploration of antigenic variation in gp120 from clades A through F of human immunodeficiency virus type 1 by using monoclonal antibodies. J. Virol 68, 8350–8364. [PubMed: 7525988]

Moore PL, Crooks ET, Porter L, Zhu P, Cayanan CS, Grise H, Corcoran P, Zwick MB, Franti M, Morris L, et al. (2006). Nature of nonfunctional envelope proteins on the surface of human immunodeficiency virus type 1. J. Virol 80, 2515–2528. [PubMed: 16474158]

Moore PL, Gray ES, Sheward D, Madiga M, Ranchobe N, Lai Z, Honnen WJ, Nonyane M, Tumba N, Hermanus T, et al.; CAPRISA 002 Study (2011). Potent and broad neutralization of HIV-1 subtype C by plasma antibodies targeting a quaternary epitope including residues in the V2 loop. J. Virol 85, 3128–3141. [PubMed: 21270156]

Morris L, Chen X, Alam M, Tomaras G, Zhang R, Marshall DJ, Chen B, Parks R, Foulger A, Jaeger F, et al. (2011). Isolation of a human antiHIV gp41 membrane proximal region neutralizing antibody by antigen-specific single B cell sorting. PLoS ONE 6, e23532. [PubMed: 21980336]

Nicely NI, Wiehe K, Kepler TB, Jaeger FH, Dennison SM, Rerks-Ngarm S, Nitayaphan S, Pitisuttithum P, Kaewkungwal J, Robb ML, et al. (2015). Structural analysis of the unmutated ancestor of the HIV-1 envelope V2 region antibody CH58 isolated from an RV144 vaccine efficacy trial vaccinee. EBioMedicine 2, 713–722. [PubMed: 26288844]

Pan R, Gorny MK, Zolla-Pazner S, and Kong XP (2015). The V1V2 region of HIV-1 gp120 forms a five-stranded beta barrel. J. Virol 89, 8003–8010. [PubMed: 26018158]

Pancera M, Zhou T, Druz A, Georgiev IS, Soto C, Gorman J, Huang J, Acharya P, Chuang GY, Ofek G, et al. (2014). Structure and immune recognition of trimeric pre-fusion HIV-1 Env. Nature 514, 455–461. [PubMed: 25296255]

Pollara J, Bonsignori M, Moody MA, Liu P, Alam SM, Hwang KK, Gurley TC, Kozink DM, Armand LC, Marshall DJ, et al. (2014). HIV-1 vaccine-induced C1 and V2 Env-specific antibodies synergize for increased antiviral activities. J. Virol 88, 7715–7726. [PubMed: 24807721]

Pollara L, Hart F, Brewer J, Pickeral B, Packard BZ, Hoxie JA, Komoriya A, Ochsenbauer C, Kappes JC, Roederer M, et al. (2011). Highthroughput quantitative analysis of HIV-1 and SIV-specific ADCC-mediating antibody responses. Cytometry A. 79, 603–612. [PubMed: 21735545]

Rerks-Ngarm S, Pitisuttithum P, Nitayaphan S, Kaewkungwal J, Chiu J, Paris R, Premsri N, Namwat C, de Souza M, Adams E, et al.; MOPH-TAVEG Investigators (2009). Vaccination with ALVAC and AIDSVAXto prevent HIV-1 infection in Thailand. N. Engl. J. Med 361, 2209–2220. [PubMed: 19843557]

Richardson SI, Chung AW, Natarajan H, Mabvakure B, Mkhize NN, Garrett N, Abdool Karim S, Moore PL, Ackerman ME, Alter G, and Morris L (2018). HIV-specific Fc effector function early in infection predicts the development of broadly neutralizing antibodies. PLoS Pathog. 14, e1006987. [PubMed: 29630668]

Rolland M, Edlefsen PT, Larsen BB, Tovanabutra S, Sanders-Buell E, Hertz T, deCamp AC, Carrico C, Menis S, Magaret CA, et al. (2012). Increased HIV-1 vaccine efficacy against viruses with genetic signatures in Env V2. Nature 490, 417–420. [PubMed: 22960785]

Scheepers C, Shrestha RK, Lambson BE, Jackson KJ, Wright IA, Naicker D, Goosen M, Berrie L, Ismail A, Garrett N, et al. (2015). Ability to develop broadly neutralizing HIV-1 antibodies is not restricted by the germline Ig gene repertoire. J. Immunol 194, 4371–4378. [PubMed: 25825450]

Schramm CA, Sheng Z, Zhang Z, Mascola JR, Kwong PD, and Shapiro L (2016). SONAR: a high-throughput pipeline for inferring antibody ontogenies from longitudinal sequencing of B cell transcripts. Front. Immunol 7, 372. [PubMed: 27708645]

Shields RL, Namenuk AK, Hong K, Meng YG, Rae J, Briggs J, Xie D, Lai J, Stadlen A, Li B, et al. (2001). High resolution mapping of the binding site on human IgG1 for Fc gamma RI, Fc gamma RII, Fc gamma RIII, and FcRn and design of IgG1 variants with improved binding to the Fc gamma R. J. Biol. Chem 276, 6591–6604. [PubMed: 11096108]

Tamura K, Stecher G, Peterson D, Filipski A, and Kumar S (2013). MEGA6: Molecular Evolutionary Genetics Analysis version 6.0. Mol. Biol. Evol 30, 2725–2729. [PubMed: 24132122]

Trkola A, Matthews J, Gordon C, Ketas T, and Moore JP (1999). A cell line-based neutralization assay for primary human immunodeficiency virus type 1 isolates that use either the CCR5 or the CXCR4 coreceptor. J. Virol 73, 8966–8974. [PubMed: 10516002]

van Loggerenberg F, Mlisana K, Williamson C, Auld SC, Morris L, Gray CM, Abdool Karim Q, Grobler A, Barnabas N, Iriogbe I, and Abdool Karim SS; CAPRISA 002 Acute Infection Study Team (2008). Establishing a cohort at high risk of HIV infection in South Africa: challenges and experiences of the CAPRISA 002 acute infection study. PLoS One 3, e1954. [PubMed: 18414658]

Walker LM, Phogat SK, Chan-Hui PY, Wagner D, Phung P, Goss JL, Wrin T, Simek MD, Fling S, Mitcham JL, et al.; Protocol G Principal Investigators (2009). Broad and potent neutralizing antibodies from an African donor reveal a new HIV-1 vaccine target. Science 326, 285–289. [PubMed: 19729618]

Wibmer CK, Bhiman JN, Gray ES, Tumba N, Abdool Karim SS, Williamson C, Morris L, and Moore PL (2013). Viral escape from HIV-1 neutralizing antibodies drives increased plasma neutralization breadth through sequential recognition of multiple epitopes and immunotypes. PLoS Pathog. 9, e1003738. [PubMed: 24204277]

Wibmer CK, Moore PL, and Morris L (2015). HIV broadly neutralizing antibody targets. Curr. Opin. HIV AIDS 10, 135–143. [PubMed: 25760932]

Wiehe K, Easterhoff D, Luo K, Nicely NI, Bradley T, Jaeger FH, Dennison SM, Zhang R, Lloyd KE, Stolarchuk C, et al. (2014). Antibody light-chain-restricted recognition of the site of immune pressure in the RV144 HIV-1 vaccine trial is phylogenetically conserved. Immunity 41, 909–918. [PubMed: 25526306]

Wiehe K, Nicely NI, Lockwood B, Kuraoka M, Anasti K, Arora S, Bowman CM, Stolarchuk C, Parks R, Lloyd KE, et al. (2017). Immunodominance of antibody recognition of the HIV envelope V2 region in Ig-humanized mice. J. Immunol 198, 1047–1055. [PubMed: 28011932]

Wu X, Yang ZY, Li Y, Hogerkorp CM, Schief WR, Seaman MS, Zhou T, Schmidt SD, Wu L, Xu L, et al. (2010). Rational design of envelope identifies broadly neutralizing human monoclonal antibodies to HIV-1. Science 329,856–861. [PubMed: 20616233]

Zhang J, Kobert K, Flouri T, and Stamatakis A (2014). PEAR: a fast and accurate Illumina Paired-End reAd mergeR. Bioinformatics 30, 614–620. [PubMed: 24142950]

Highlights

- V2-specific antibodies from HIV infection that resemble vaccine-elicited antibodies

- Use of a different antibody light chain with a different V2 K169-binding motif

- Show broad ADCC activity against globally relevant V2 immunotypes

- Increases the repertoire of B cells able to respond to RV144 V2 immunogens
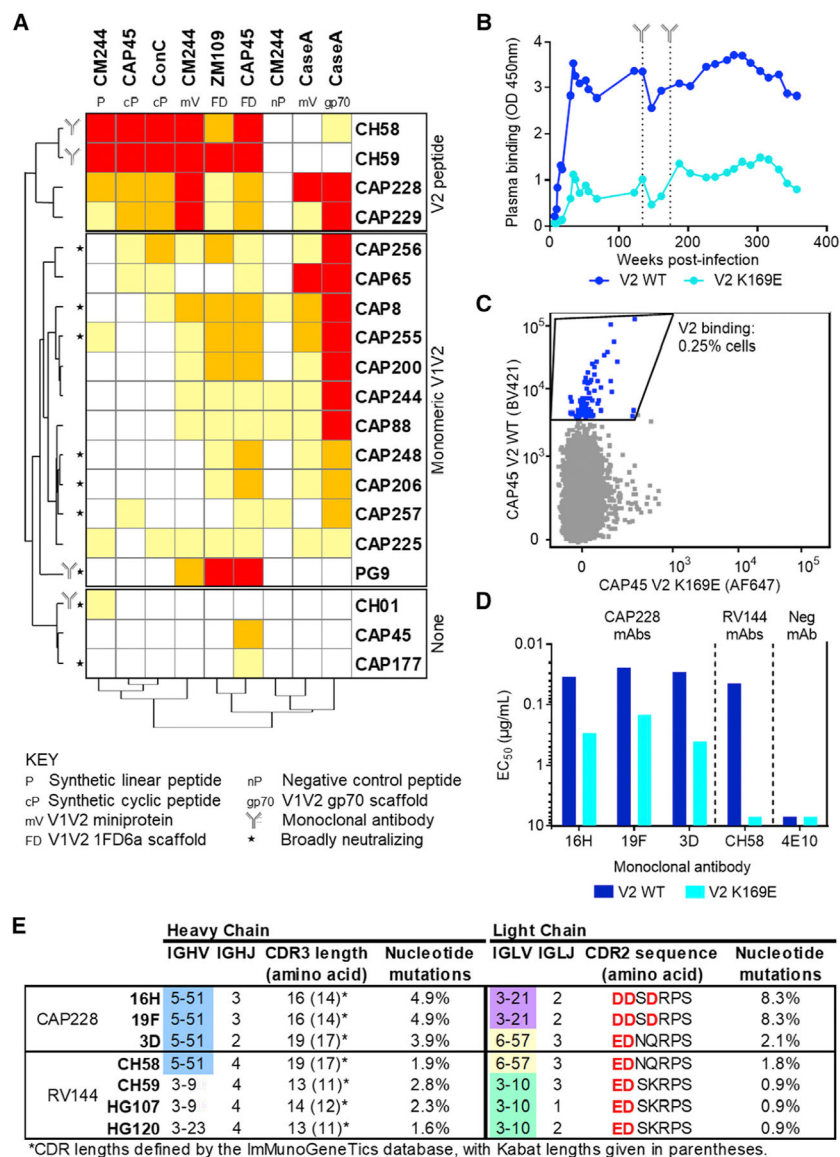
Figure 1. Isolation of V2p-Binding Antibodies from an HIV-1-Infected Donor

(A)Hierarchical clustering of 15 HIV-1 + plasma samples and four anti-V2 mAbs (labeled on the right) based on their relative reactivity with V2 peptides or scaffolded V1V2 antigens (labeled on the top and in the key) in an ELISA. Plasma samples and mAbs with broadly neutralizing activity are indicated with an asterisk on the left-hand side. Binding intensity was recorded as a relative percentage of maximum OD, where 0%–40% was colored yellow; 40%–80%, orange; and 80%–100%, red. Samples were grouped either with mAbs CH58 and CH59 (based on strong binding to peptides), with PG9 (based on binding to monomeric V1V2 proteins), or with CH01 (based on no/limited binding to the peptides or proteins).

(b) ELISA binding of CAP228 longitudinal plasma to CAP45 wild-type (blue) and K169E mutant (cyan) cyclical V2 peptides. Absorbance readings are plotted on the y axis against time on the x axis. The 134 and 174 wpi time points at which mAbs were isolated from stored PBMC samples are indicated with the vertical dotted lines.

(C) Fluorescence-activated cell sorting (FACS) plot showing the CAP228 memory B cells (in blue) that bind BV421-labeled wild-type (y axis), but not AF647-labeled K169E mutant (x axis) V2 peptide antigens, and were therefore sorted for PCR amplification.

(D)ELISA titers (y axis) of three CAP228 mAbs (16H, 19F, and 3D) to both wild-type and K169E mutant V2 peptides from CAP45 (colored as in B), when compared to the RV144 vaccine antibody CH58 (CH59 did not bind to CAP45 V2 peptides). 4E10 is an HIV-1 gp41 peptide-reactive mAb used as a negative control (Buchacher et al., 1994).

(E) Properties of the CAP228 antibodies, defined by the International Immunogenetics Database (IMGT), compared to vaccine-elicited mAbs CH58 and CH59. CDRH3 lengths are also given for Kabat numbering in parentheses. Shared immunoglobulin germline genes are shaded, and the negatively charged amino acids in each CDRL2 are shown in red.
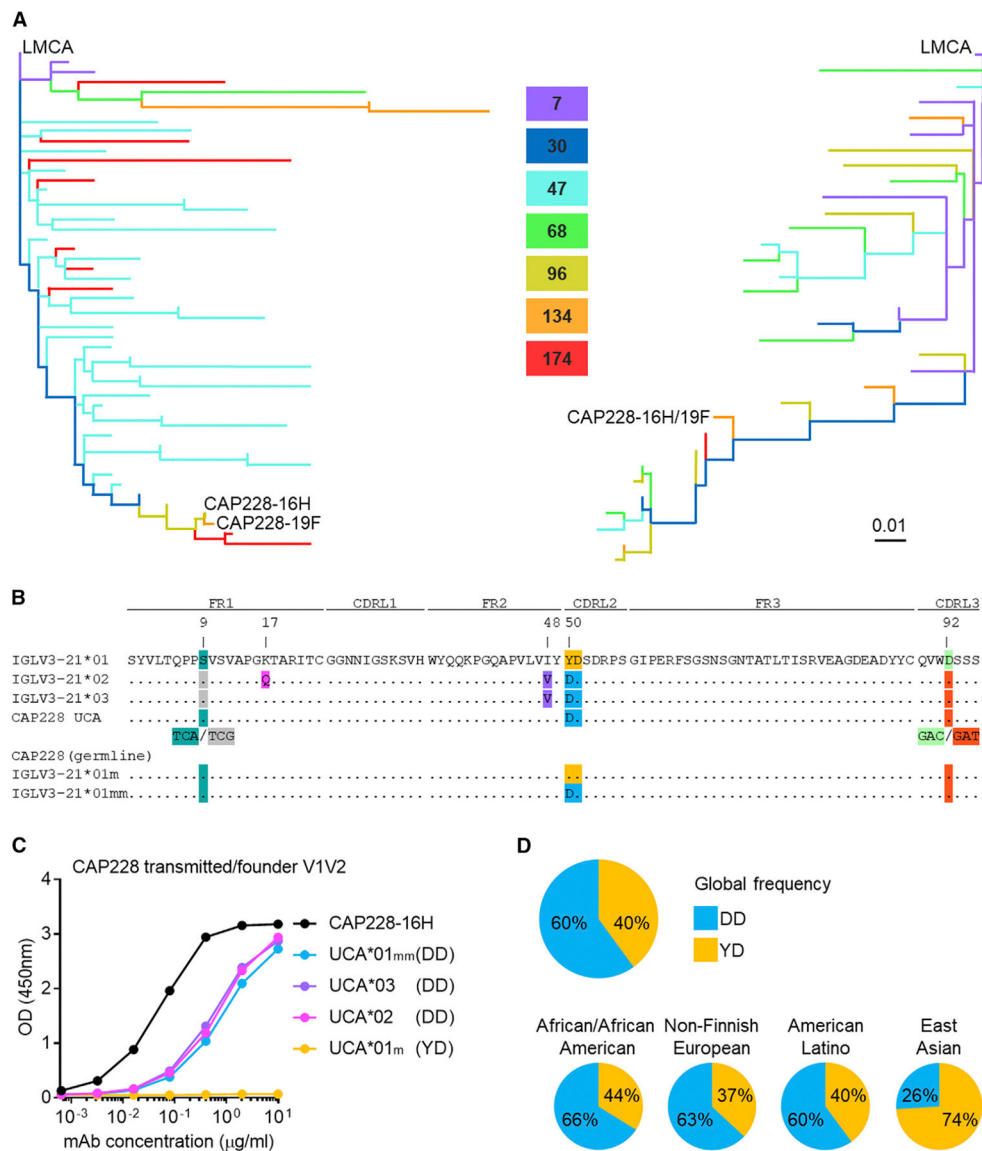
Figure 2. Identification of the CAP228-16H/19F UCA and Lambda IGLV3–21 Germline Alleles

(A) Maximum-likelihood phylogenetic trees of unique, clonally related sequences, for the heavy (left) and light (right) chain of the CAP228-16H/19F lineage, with branches colored by time point. Mature CAP228-16H and 19F mAb sequences are colored according to the time point at which they were first observed rather than when they were isolated. Trees were rooted to the least mutated common ancestor (LMCA).

(b) Alignment of the two additional CAP228 IGLV3–21 germline alleles, when compared to the IMGT sequences for IGLV3–21*01, IGLV3–21*02, and IGLV3–21*03. Shared synonymous (positions 9 or 92) and non-synonymous (positions 17, 48, or 50) differences are indicated with alternate shading, where the key YD/DD amino acid pair is colored yellow or blue, respectively.

(C) ELISA binding of the CAP228-16H/19F UCA to an autologous transmitted/founder CAP228 V1V2 scaffolded protein. Absorbance readings are plotted on the y axis versus

mAb concentration on the x axis. Binding of the CAP228-16H/19F UCA allelic variants for IGLV3–21*02 (pink) and IGLV3–21*03 (purple) are also shown. IGLV3–21*01 shares the same amino acid sequence as IGLV3–21*01m.

(D) Frequency of the DD (blue) or YD (yellow) motifs among global allelic variants of the IGVL3–21 germline genes (data from The 1000 Genomes Project [Auton et al., 2015]).
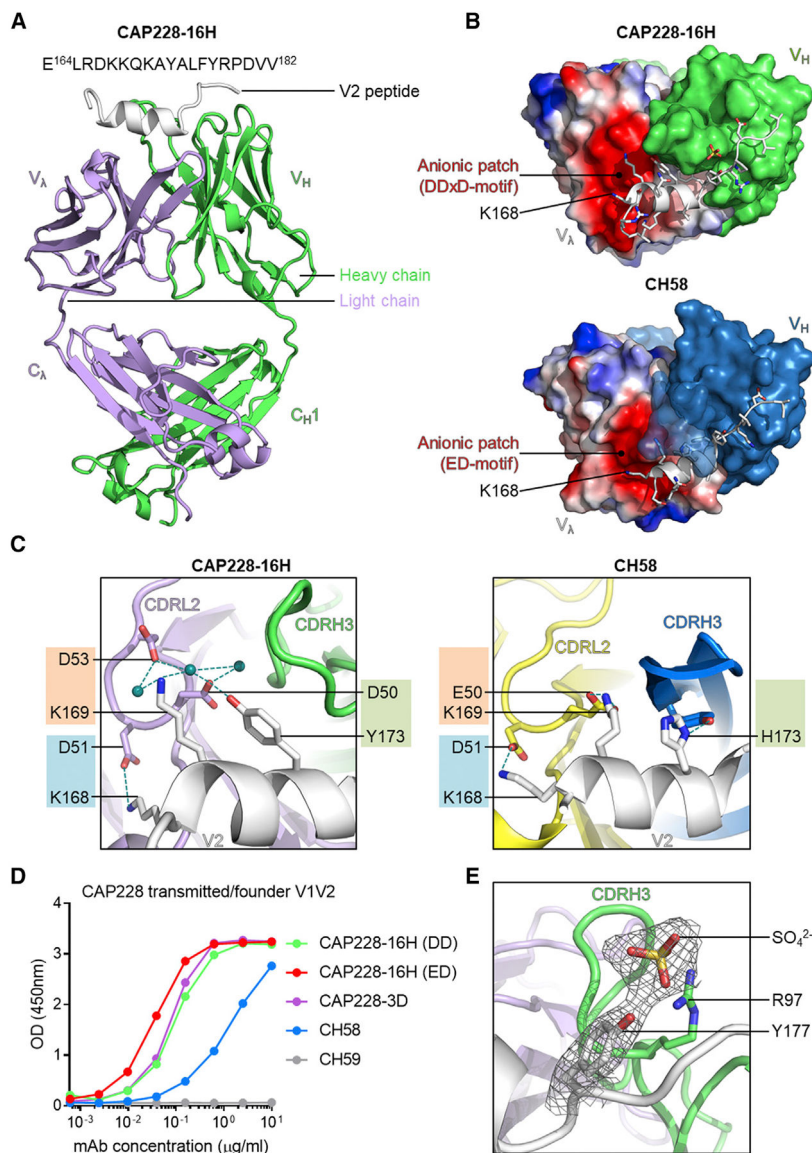
Figure 3. Atomic-Level Details of the Interaction between CAP228-16H and V2 Residues

(A) Cartoon representation of the CAP228-16H Fab domain bound to V2 peptide residues 164–182 from viral strain CAP45 (colored white). Heavy and light chains are colored green and purple, respectively, and the variable or constant domains of the Fab are labeled.

(B) Surface representation of the CAP228-16H paratope (top), compared to the CH58 paratope (bottom), with the bound V2 peptide depicted as a helix-loop cartoon with side chains shown in stick representation. The Fab heavy chains are colored green and blue, respectively, while the light chains are colored per electrostatic potential. The CH58 CDRH3 was colored with partial transparency to show the underlying V2 peptide. The large electronegative patch encoded by the IGLV3–21 DDxD motif, or the IGLV6–57 ED motif, is indicated, and K168 in V2 is labeled for perspective.

(C) A zoom-in of the atomic detail interactions (shown with side chain sticks) between V2 residues K168, K169, and Y/H173, and the CAP228– 16H light chain DDxD or CH58 ED

motifs. Hydrogen bonds are indicated with the dotted lines, and water molecules are shown with the blue spheres. The antibody CDRL2 and CDRH3 loops, as well as the interacting amino acid pairs being compared, are labeled.

(D) ELISA showing binding to the autologous transmitted/founder CAP228 V1V2 scaffolded protein by wild-type CAP228-16H (green), and the ED-motif mutant (red), when compared to antibodies that naturally contain the ED motif: CAP228–3D (purple), CH58 (blue), and CH59 (gray). Absorbance readings are plotted on the y axis versus mAb concentration on the x axis.

(E) 2Fo-Fc density map of V2 residue Y177, showing the associated sulfate ion, oriented by CAP228-16H CDRH3 residue R97.

Figure 4. Increased V2 Coverage and Broader ADCC Activity Mediated by CAP228 Antibodies

(A) Buried surface area for V2 peptides residues 165–182 (x axis) from the CAP228-16H (purple) or CH58 (green) cocrystal structures, plotted as a percentage of the total accessible surface area (y axis). Significant differences between the two structures are boxed in yellow, and hydrogen bonds (H) or salt bridges (S) are labeled. The potential interaction between CAP228-16H and a sulfated tyrosine at position Y177 is indicated with the asterisk.
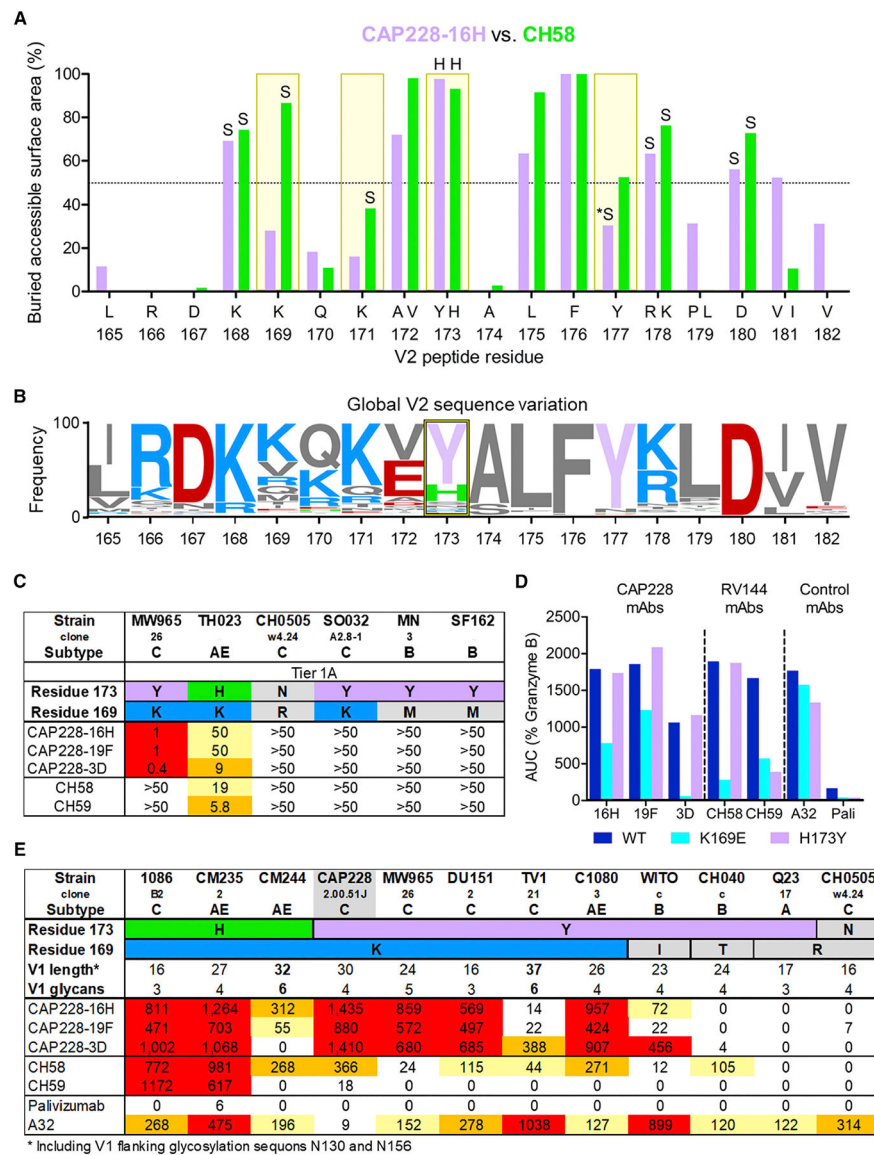
(B) Global frequency (y axis) of amino acids occurring at V2 positions 165–182 (x axis), from non-redundant sequences in the HIV-1 Los Alamos National Laboratory (LANL) database, aligned with V2 residues in (A). Positively or negatively charged residues are colored blue or red, while the tyrosines recognized by CAP228-16H, and the histidine required for CH58 are colored purple and green, respectively. Position 173 is boxed in yellow.

Panel C

Strain clone Subtype	MW965 26 C	TH023 AE	CH0505 w4.24 C	SO032 A2.8-1 C	MN 3 B	SF162 B
			Tier 1A			
Residue 173	Y	H	N	Y	Y	Y
Residue 169	K	K	R	K	M	M
CAP228-16H	1	50	>50	>50	>50	>50
CAP228-19F	1	50	>50	>50	>50	>50
CAP228-3D	0.4	9	>50	>50	>50	>50
CH58	>50	19	>50	>50	>50	>50
CH59	>50	5.8	>50	>50	>50	>50

Panel E

Strain clone Subtype	1086 B2 C	CM235 2 AE	CM244 AE	CAP228 2.00.51J C	MW965 26 C	DU151 2 C	TV1 21 C	C1080 3 C	WITO c B	CH040 c B	Q23 17 A	CH0505 w4.24 C
Residue 173		H		Y								N
Residue 169			K						I	T	R	
V1 length*	16	27	32	30	24	16	37	26	23	24	17	16
V1 glycans	3	4	6	4	5	3	6	4	4	4	3	4
CAP228-16H	811	1,264	312	1,435	859	569	14	957	72	0	0	0
CAP228-19F	471	703	55	880	572	497	22	424	22	0	0	7
CAP228-3D	1,002	1,068	0	1,410	680	685	388	907	456	4	0	0
CH58	772	981	268	366	24	115	44	271	12	105	0	0
CH59	1172	617	0	18	0	0	0	0	0	0	0	0
Palivizumab	0	6	0	0	0	0	0	0	0	0	0	0
A32	268	475	196	9	152	278	1038	127	899	120	122	314

* Including V1 flanking glycosylation sequons N130 and N156

(C) Neutralization activity of the CAP228 mAbs, or RV144 mAbs CH58 and CH59, in the TZM-bl assay against six tier 1A HIV-1 viruses. IC_{50} titers 1 μg/mL were colored red, while those between 1 and 10 μg/mL are shown in orange, and those between 10 and 50 μg/mL are shown in yellow.

(D) Mapping the V2-directed ADCC activity by the granzyme B assay against HIV-1 1086 gp120-coated target cells. Measurements represent area under the curve (y axis) for wild-type (blue), K169E (cyan), or H173Y (purple) mutant proteins.

(E) ADCC activity of the CAP228 mAbs against CEM.NKR-CCR5 cells infected with a multi-clade panel of 12 HIV-1 strains, compared to CH58 and CH59. Data report percentage activity versus antibody concentration as area under the curve, above 15% background, and are displayed as a heatmap with >400 shown in red; 200–400, in orange; 40–200, in yellow; and <40, in white. Relevant genotypic information for each envelope strain is also shown, grouped according to immunotypes at residues 169 and 173. The mAb A32 with known ADCC activity was included as a positive control and showed reactivity against all infected cells, while Palivizumab (a non-HIV antibody) was included as a negative control.

Table 1.

X-Ray Crystallographic Data and Refinement Statistics (Molecular Replacement) for the Antigen-Binding Fragment of CAP228-16H in Complex with HIV-1 CAP45 V2 Peptide

	CAP228-16H Bound to CAP45 V2 Peptide
Data Collection	
Space group	$P2_12_12_1$
Cell dimensions	
a, b, c (Å)	40.29, 104.27, 212.22
α, β, γ (°)	90, 90, 90
Resolution (Å)	35.37–2.58 (2.67–2.58)[a]
Unique reflections	26,374 (1,710)
R_{merge}	0.158 (0.373)[a]
R_{pim}	0.068 (0.263)[a]
$I/\sigma I$	10.4 (2.1)[a]
CC1/2	0.951 (0.873)[a]
Completeness (%)	90.2 (59.4)[a]
Redundancy	5.1 (2.5)[a]
Refinement	
Resolution (Å)	50–2.58
No. reflections	26,364 (1,709)
R_{work}/R_{free}	0.22/0.25
No. atoms (no H)	6.922
Protein	6,786
Other	20
Solvent	116
B factors (no H)	72
Protein	72
Other	87
Solvent	53
Wilson B-factor (Å^2), all atoms	54
RMS deviations	
Bond lengths (Å)	0.003
Bond angles (°)	0.650
Ramachandran favored %	96.5%
Ramachandran outliers %	0.0%
Rotamer outliers %	0.1%
Molprobity clash score	1.5
MolProbity overall score	1.0
PDB ID	6FY0

[a] Values in parentheses are for highest-resolution shells.

KEY RESOURCES TABLE

REAGENT or RESOURGE	SOURGE	IDENTIFIER
Antibodies		
CH58 expressed as IgG1 or 3A variant	(Liao et al., 2013)	Expressed in-house
CH59 expressed as IgG1 or 3A variant	(Liao et al., 2013)	Expressed in-house
PG9 expressed as IgG1	(Walker et al., 2009)	Expressed in-house
CH01 expressed as IgG1	(Bonsignori et al., 2011)	Expressed in-house
4E10 expressed as IgG1	(Buchacher et al., 1994)	Expressed in-house
A32 expressed as IgG1 variants	(Moore et al., 1994)	Expressed in-house
CAP228-16H expressed as IgG1 or 3A variant	This study	Expressed in-house
CAP228–19F expressed as IgG1 or 3A variant	This study	Expressed in-house
CAP228–3D expressed as IgG1 or 3A variant	This study	Expressed in-house
CAP228-16H/19F UCA allele *01mm expressed as IgG1	This study	Expressed in-house
CAP228-16H/19F UCA allele *02 expressed as IgG1	This study	Expressed in-house
CAP228-16H/19F UCA allele *02 expressed as IgG1	This study	Expressed in-house
CAP228-16H/19F UCA allele *01m expressed as IgG1	This study	Expressed in-house
CAP228-16H D50E (ED) mutant expressed as IgG1	This study	Expressed in-house
Palivizumab (Synagis®)	MedImmune	RRID: AB_2459638
Mouse anti-CD3 phycoerythrin conjugate	BD Biosciences	CAT#555340
Mouse anti-CD14 phycoerythrin conjugate	BD Biosciences	CAT#562691
Mouse anti-CD16 phycoerythrin conjugate	BD Biosciences	CAT#555407
Mouse anti-IgD Fluorescein isothiocyanate conjugate	BD Biosciences	CAT#555778
Bacterial and Virus Strains		
One Shot™ TOPIO Chemically Competent *E. coli*	Thermo Fisher Scientific	GAT#G4040
XL10-Gold® Ultracompetent Cells	Stratagene	GAT#200315
MAX Efficiency Stbl2 Competent Cells	Thermo Fisher Scientific	GAT#10268019
HIV-1 strain TH023	http://www.hiv.lanl.govcontent/index	GenBank KU562843
HIV-1 strain SO032.A2.8-C1	http://www.hiv.lanl.govcontent/index	GenBank KF114894
HIV-1 strain MN.3	http://www.hiv.lanl.govcontent/index	GenBank HM215430
HIV-1 strain SF162	http://www.hiv.lanl.govcontent/index	GenBank EU123924
HIV-1 strain 1086.B2	http://www.hiv.lanl.govcontent/index	GenBank FJ444395
HIV-1 strain CM235.2	http://www.hiv.lanl.govcontent/index	GenBank AF259954
HIV-1 strain CM244	http://www.hiv.lanl.govcontent/index	GenBank KG822429
HIV-1 strain CAP228.2.00.51J	http://www.hiv.lanl.govcontent/index	GenBank EF203968
HIV-1 strain MW965.26	http://www.hiv.lanl.govcontent/index	GenBank U08455
HIV-1 strain DU151.2	http://www.hiv.lanl.govcontent/index	GenBank DQ411851
HIV-1 strain TV1.21	http://www.hiv.lanl.govcontent/index	GenBank HM215437

REAGENT or RESOURGE	SOURGE	IDENTIFIER
HIV-1 strain C1080.3	http://www.hiv.lanl.govcontent/index	GenBank JN944660
HIV-1 strain WITO.c	http://www.hiv.lanl.govcontent/index	GenBank JN944948
HIV-1 strain CH040.c	http://www.hiv.lanl.govcontent/index	GenBank JN944939
HIV-1 strain Q23.17	http://www.hiv.lanl.govcontent/index	GenBank AF004885
HIV-1 strain CH0505.w4.24	http://www.hiv.lanl.govcontent/index	GenBank KG247577
HIV-1 strain ZM109	http://www.hiv.lanl.govcontent/index	GenBank AY424138
Biological Samples		
GAPRISA 002 Acute Infection study plasma and PBMG	(van Loggerenberg et al., 2008)	Processed in-house
HIV-1 negative PBMG	RSA National Blood Service	Case-by-case
Chemicals, Peptides, and Recombinant Proteins		
Streptavidin Brilliant Violet 421 conjugate	Biolegend	CAT#405226
Streptavidin AlexaFlour 647 conjugate	Life Technologies	CAT#S32357
CAP228.2.00.51J V1V2 1FD6 scaffold	This study	Expressed in-house
HIV-1 strain CAP45.2.00.G3 V1V2 1FD6 scaffold	(McLellan etal., 2011)	Expressed in-house
HIV-1 strain ZM109 V1V2 1FD6 scaffold	(McLellan etal., 2011)	Expressed in-house
HIV-1 strain CAP45.2.00.G3 V2 synthetic peptide	This study	Synthesized
HIV-1 clade C consensus V2 synthetic peptide	This study	Synthesized
HIV-1 strain CM244 negative control peptide	(Haynes et al., 2012)	Synthesized
HIV-1 strain CM244 synthetic linear peptide	(Haynes et al., 2012)	Synthesized
HIV-1 strain CM244 V1V2 miniprotein	(Haynes et al., 2012)	Expressed in-house
HIV-1 caseA strain V1V2 miniprotein	(Haynes et al., 2012)	Expressed in-house
HIV-1 case A strain V1V2 gp70 scaffold	(Haynes et al., 2012)	Expressed in-house
SuperScript III Reverse Transcriptase	Thermo Fisher Scientific	CAT#18080
HotStarTaq DNA Polymerase	QIAGEN	CAT#203207
Critical Commercial Assays		
ZEUS AtheNA Multi-Lyte® ANA-II Plus Test SystemData described in Table S2	Zeus Scientific	CAT#A21101
Deposited Data		
CAP228-16H bound to CAP45 V2 peptide	This study	PDB 6FY0
CAP228-16H heavy chain variable domain sequence	This study	GenBank: MK119167
CAP228–19F heavy chain variable domain sequence	This study	GenBank: MK119168
CAP228-16H/19F light chain variable domain sequence	This study	GenBank: MK119169
CAP228–3D heavy chain variable domain sequence	This study	GenBank: MK119170
CAP228–3D light chain variable domain sequence	This study	GenBank: MK119171
Variable domain sequencing of heavy and light chain genes from both CAP228-16H/19F and CAP228–3D V2p antibody lineages	This study	SRA: PRJNA498753 Accession codes: SAMN10334092 to SAMN10334110
Experimental Models: Cell Lines		
HEK293T/17 cells	NIH AIDS Reagent Program	ATCC CRL-11268
FreeStyle 293-F cells	Thermo Fisher Scientific	CAT#R79007
HEK293S N-acetylglucosaminyltransferase I(–/–) cells	NIH AIDS Reagent Program	ATCC CRL-3022
CEM.NKR CCR5+ cells	NIH AIDS Reagent Program	CAT#4376
Oligonucleotides		

REAGENT or RESOURGE	SOURGE	IDENTIFIER
Listed in Tables S4 and S5	This study	Synthesized
Software and Algorithms		
FlowJo	Tree Star	RRID: SCR_008520
PEAR	(Zhang et al., 2014)	RRID: SCR_003776
USEARCH	(Edgar, 2010)	RRID: SCR_006785
SONAR bioinformatics pipeline	(Schramm et al., 2016)	https://github.com/scharch/SONAR
MEGA 6	(Tamura et al., 2013)	RRID: SCR_000667
PhyML 3.0	(Guindon et al., 2010)	RRID: SCR_014629
Dendroscope	(Huson and Scornavacca, 2012)	http://danielhuson.github.io/dendroscope3/
PHENIX suite	(Adams et al., 2010)	RRID: SCR_014224
Coot	(Emsley et al., 2010)	RRID: SCR_014222
PyMOL Molecular Graphics System	(Schrodinger LLC)	RRID: SCR 000305